

Evaluation of the Theoretical Uncertainties in the $W \rightarrow \ell\nu$ Cross Sections at the LHC

Nadia E. Adam,^a Valerie Halyo,^a Scott A. Yost,^b and Wenhan Zhu^a

^a*Department of Physics, Princeton University, Princeton, NJ 08544 USA*

^b*Department of Physics, The Citadel, Charleston SC 29409 USA*

E-mail: neadam@princeton.edu, valerieh@princeton.edu,
scott.yost@citadel.edu, wenhanz@princeton.edu

ABSTRACT: We study the sources of systematic errors in the measurement of the $W \rightarrow \ell\nu$ cross-sections at the LHC. We consider the systematic errors in both the total cross-section and acceptance for anticipated experimental cuts. We include the best available analysis of QCD effects at NNLO in assessing the effect of higher order corrections and PDF and scale uncertainties on the theoretical acceptance. In addition, we evaluate the error due to missing NLO electroweak corrections and propose which MC generators and computational schemes should be implemented to best simulate the events.

KEYWORDS: Hadronic Colliders, NLO Computations, QCD.

Contents

1. Introduction	1
2. Theoretical Calculations and MC Generators	2
3. Electroweak Corrections	4
4. NNLO QCD Uncertainties	5
5. Scale Dependence	10
6. Uncertainties Due to the Parton Distribution Function	13
7. Conclusions	16

1. Introduction

A precise measurement of gauge boson production cross-sections for pp scattering will be crucial at the LHC. W and Z bosons will be produced copiously, and a careful measurement of their production cross-sections will be important in testing the Standard Model more rigorously than ever before, and uncovering signs of new physics which may appear through radiative corrections. In addition, these cross-sections have been proposed as a “standard candle” for measuring the luminosity through a comparison of the measured rates to the best theoretical calculations of the cross-section. Investigation of this means of measuring luminosity began at the Tevatron and will continue at the LHC [1, 2].

In a previous paper, [3] three of the authors analyzed the systematic errors in Z production using state-of-the-art computational tools. A comparable analysis of systematic uncertainties in W production appeared in Ref. [4]. Since that time, both the experimental approach to the measurements and the theoretical results needed to calculate them have both been refined, so we will extend a similar analysis as in Ref. [3] to the case of the W . As in the case of the Z , NNLO QCD calculations of these processes, previously available only for the total cross-section [5] and rapidity distribution [6], are now available in differential form [7], permitting an analysis of the effect of experimental cuts on the pseudorapidity and transverse momentum of the final state charged lepton and missing energy of the neutrino.

The high luminosity ($10^{33} - 10^{34} \text{ cm}^2\text{s}^{-1}$) at the LHC insures that systematic errors will play a dominant role in determining the accuracy of the cross-section. Thus, we present an analysis of the effect of the theoretical uncertainty in the evaluation of the acceptance, and propose which among the various available MC generators and computational schemes should be implemented to best simulate the events.

This paper is organized as follows. Sec. 2 will give an overview of the calculation and the computational tools used in the analysis. The next four sections are each devoted to estimating a class of systematic errors: electroweak corrections in Sec. 3, NNLO QCD in Sec. 4, QCD scale dependence in Sec. 5, and parton distribution function uncertainties in Sec. 6. Finally, the results are compiled and summarized in Sec. 7.

2. Theoretical Calculations and MC Generators

The dominant production mechanism for Z or W bosons is the Drell-Yan process [8], in which a quark and antiquark annihilate to form a vector boson, which subsequently decays into a lepton pair. The W production process is actually observed through the charged lepton and missing energy of the neutrino produced in its decay. In general, the cross-section may be inferred from the number N_W^{obs} of observed events via the relation

$$N_W^{\text{obs}} = \sigma^{\text{tot}} \text{BR}(W \rightarrow \ell\nu) A_W \int \mathcal{L} dt. \quad (2.1)$$

A_W is the acceptance obtained after applying the experimental selection criteria. For example, if the cuts require $p_T > p_T^{\text{min}}$, $0 < \eta^\ell < \eta_{\text{max}}$, and $\cancel{E}_T > \cancel{E}_T^{\text{min}}$, then

$$A_W(p_T^{\text{min}}, \eta_{\text{max}}) = \frac{1}{\sigma^{\text{tot}} \text{BR}(W \rightarrow \ell\nu)} \int_{p_T^{\text{min}}}^{\sqrt{s}/2} dp_T^\ell \int_{\cancel{E}_T^{\text{min}}}^{\sqrt{s}/2} dp_T^\nu \times \int_{-\eta_{\text{max}}}^{\eta_{\text{max}}} d\eta_\ell \int_{-\infty}^{\infty} d\eta_\nu \frac{d^4\sigma}{dp_T^\ell dp_T^\nu d\eta_\ell d\eta_\nu} \text{BR}(W \rightarrow \ell\nu), \quad (2.2)$$

Alternatively to the W production cross-section measurement, the corrected W yield can be used as a standard candle for a luminosity monitor in LHC if one calculates the cross-section and solves for $\int \mathcal{L} dt$. The theoretical cross-section may be constructed by convoluting a parton-level cross-section $\hat{\sigma}_{ab}$ for partons a and b with the parton density functions (PDFs) f_a , f_b for these partons,

$$\sigma^{\text{th}} \text{BR}(W \rightarrow \ell\nu) = \sum_{a,b} \int_0^1 dx_1 dx_2 f_a(x_1) f_b(x_2) \hat{\sigma}_{ab}(x_1, x_2), \quad (2.3)$$

integrating over the momentum fractions x_1, x_2 , and applying cuts relevant to the experiment. Theoretical errors come from limitations in the order of the calculation of σ_{ab} , on its completeness (for example, on whether it includes electroweak corrections, on whether any phase space variables or spins have been averaged), and from errors in the PDFs.

Since the final state may include additional partons which form a shower, the output from the hard QCD process must be fed to a shower generator to generate a realistic final state seen in a detector. This is possible only if the cross-section is simulated in an event generator. Calculating the acceptance for all but the simplest cuts will normally require an event generator as well.

Thus, when constructing a simulation of an experiment, there is a range of choices which can be made among the tools currently available. An efficient calculation requires

selecting those adequate to meet the anticipated precision requirements, without performing unnecessarily complex calculations. For example, while NNLO calculations are now available, the cross-sections are very complicated, do not always converge well, and require substantial time to calculate. For certain choices of cuts, it may be found that the effect of the NNLO result can be minimized, or that it can be represented by a simplified function for the parameters of interest. We will compare several possible schemes for calculating the W production cross-section and acceptance, and consider the systematic errors arising for these schemes.

The most basic way to generate events is through one of the showering programs, such as PYTHIA [9], HERWIG [10], ISAJET [11] or SHERPA [12]. These vary somewhat in their assumptions and range of effects included, but they all start with hard partons at a high energy scale and branch to form partons at lower scales, which permits a description of hadronization and realistic events. On their own, these programs typically rely on a leading order hard matrix element and include only a leading-log resummation of soft and collinear radiation in the shower, limiting their value in describing events with large transverse momentum. In addition, ISAJET lacks color-coherence, which is important in predicting the correct distribution of soft jets [13].

Fully exclusive NLO QCD calculations are available for W and Z boson production [14]. The MC generator MC@NLO [15] combines a parton-level NLO QCD calculation with the HERWIG [10] parton shower, thus removing some of the limitations of a showering program alone.

Since $\alpha \approx \alpha_s^2$ at LHC energies, NLO electroweak (EWK) corrections should appear at the same order as NNLO QCD. The MC@NLO package is missing EWK corrections, but the contribution of final state radiation (FSR) can be obtained by combining MC@NLO with PHOTOS [16], an add-on program which generates multi-photon emission from events created by the host program. In the case of Z exchange, FSR was expected to be the dominant contribution. [17] Another program, HORACE [18], is available which includes exact $\mathcal{O}(\alpha)$ EWK corrections together with a final state QED parton shower. It was confirmed [3] that PHOTOS and HORACE agree within 1% for Z production. However, for W production, the W itself can radiate, so we should expect that the agreement may not be so close in this case. Recent studies [19] have emphasized the importance of the interplay between QCD and EWK corrections, particularly in the high p_T tail important for new physics searches.

The other available NLO and NNLO calculations are implemented as MC integrations, which can calculate a cross-section but do not provide unweighted events. Some of these are more differential than others. For example, the NNLO rapidity distribution is available in a program Vrap [6], but this distribution alone is not sufficient to calculate acceptances with cuts on the lepton pseudorapidities and transverse momenta. A differential version of this NNLO calculation is implemented in a program FEWZ [7], but this is not an event generator. Another available program is ResBos-A [20], which resums soft and collinear initial state QCD radiation to all orders and includes NLO final state QED radiation. Resummation is expected to have advantages in realistically describing the small

p_T regime [20].

Our analysis is conducted for di-lepton final states. The available calculations typically set the lepton masses to zero, so the lepton masses will be neglected throughout this paper and the choice of final state lepton has no effect on the calculations. In all results, ℓ may be interpreted as either an electron or muon, ν the appropriate accompanying (anti)neutrino, and we consider the case of W^\pm production separately. We have chosen three sets of experimental cuts to reflect detector capabilities and to demonstrate the impact of physics effects on the acceptances depending on the selection criteria.

3. Electroweak Corrections

As noted above, both NNLO QCD corrections and NLO electroweak (EWK) corrections are expected to be needed to reach precisions on the order of 1% or better in W boson production. NLO electroweak[21] and QCD corrections[14] are known both for W boson production and Z boson production. However, current state-of-the-art MC generators do not include both sets of corrections. The generator MC@NLO [15] combines a MC event generator with NLO calculations of rates for QCD processes and uses the HERWIG event generator for the parton showering, but it does not include EWK corrections. Final state QED can be added using PHOTOS [16], a process-independent module for adding multi-photon emission to events created by a host generator. However, some $\mathcal{O}(\alpha)$ EWK corrections are still missing, in particular radiation from the charged W itself, which was not an issue in Z production.

To study the error arising from missing $\mathcal{O}(\alpha)$ EWK corrections, we used HORACE [18], a MC event generator that includes initial and final-state QED radiation in a photon shower approximation and exact $\mathcal{O}(\alpha)$ EWK corrections matched to a leading-log QED shower. To determine the magnitude of the error, we then compared the results from this generator to a Born-level calculation with final-state QED corrections added by PHOTOS.

Specifically, we compared $pp \rightarrow W \rightarrow \ell\nu$ events generated by HORACE with the full $\mathcal{O}(\alpha)$ corrections and parton-showered with HERWIG, to these events generated again by HORACE, but without EWK corrections (Born-level), showered with HERWIG+PHOTOS. CTEQ6.5M parton distribution functions [22] were used in the calculations. The results are shown in Tables 2 – 3 and in Figs. 1 – 3.

For Tables 2 – 3, a standard set of cuts is used. We choose three sets of experimental cuts described in Table 1 to reflect detector capabilities and to demonstrate the impact of physics effects on the acceptances depending on the selection criteria. Here, η and p_T are the pseudorapidity and transverse momentum of the final state charged leptons, and \cancel{E}_T is the missing transverse energy carried by the neutrino. The different cuts provide useful separation for between regions of the W spectrum which have different sensitivities to some of the sources of uncertainties.

The first row in the table shows the total generator-level cross-sections before QCD parton showering (identified by the label “Total”). The Born+FSR column shows the effect of applying final state radiation (FSR) corrections only via PHOTOS. In PHOTOS, FSR affects the rates through the cuts only.

	Transverse Momentum (GeV/c)	Pseudorapidity	Missing Transverse Energy (GeV)
Cut 1	$p_T > 25$	$ \eta < 1$	$\cancel{E}_T > 20$
Cut 2	$p_T > 25$	$1 < \eta < 2.2$	$\cancel{E}_T > 20$
Cut 3	$p_T > 25$	$ \eta < 1$	$\cancel{E}_T > 30$

Table 1: Acceptance regions for the Electroweak and NNLO studies

Photonic and Electroweak Corrections: W^+ Production

	Born	Born+FSR	ElectroWeak	Difference
σ (Total)	10780.6 ± 1.2	10780.6 ± 1.2	11201.4 ± 1.6	$3.90 \pm 0.02\%$
σ (Cut 1)	1321.3 ± 5.4	1294.0 ± 5.4	1345.8 ± 5.6	$4.00 \pm 0.61\%$
σ (Cut 2)	1639.1 ± 5.9	1604.7 ± 5.9	1656.7 ± 6.1	$3.24 \pm 0.53\%$
σ (Cut 3)	1008.9 ± 4.9	989.0 ± 4.8	1023.1 ± 5.0	$3.45 \pm 0.71\%$
A (Cut 1)	0.1652 ± 0.0007	0.1618 ± 0.0007	0.1619 ± 0.0007	$0.09 \pm 0.59\%$
A (Cut 2)	0.2049 ± 0.0007	0.2006 ± 0.0007	0.1993 ± 0.0007	$-0.64 \pm 0.51\%$
A (Cut 3)	0.1261 ± 0.0006	0.1236 ± 0.0006	0.1231 ± 0.0006	$-0.44 \pm 0.69\%$

Table 2: Calculation of the $W^+ \rightarrow \ell^+ \nu_\ell$ cross-section σ and acceptance A for various EWK corrections generated using HORACE 3.1, for $\ell = e$ or μ .

Photonic and Electroweak Corrections: W^- Production

	Born	Born+FSR	ElectroWeak	Difference
σ (Total)	7998.1 ± 1.1	7998.1 ± 1.1	8311.3 ± 2.6	$3.92 \pm 0.04\%$
σ (Cut 1)	1498.5 ± 5.7	1466.7 ± 5.7	1524.1 ± 5.9	$3.91 \pm 0.57\%$
σ (Cut 2)	1611.0 ± 5.9	1578.8 ± 5.8	1648.5 ± 6.1	$4.41 \pm 0.54\%$
σ (Cut 3)	1158.9 ± 5.1	1135.4 ± 5.1	1180.6 ± 5.3	$3.98 \pm 0.66\%$
A (Cut 1)	0.1873 ± 0.0007	0.1833 ± 0.0007	0.1834 ± 0.0007	$0.05 \pm 0.54\%$
A (Cut 2)	0.2014 ± 0.0007	0.1974 ± 0.0007	0.1983 ± 0.0007	$0.46 \pm 0.50\%$
A (Cut 3)	0.1449 ± 0.0006	0.1419 ± 0.0006	0.1420 ± 0.0006	$0.07 \pm 0.60\%$

Table 3: Calculation of the $W^- \rightarrow \ell^- \bar{\nu}_\ell$ cross-section σ and acceptance A for various EWK corrections generated using HORACE 3.1, for $\ell = e$ or μ .

The ElectroWeak column includes the full HORACE EWK corrections. In the final column, we give the difference between the previous two columns, to compare the full EWK correction FSR alone. The cross-section (acceptance) results show agreement within 4% (0.7 %) between the two schemes. The maximum error in the cross-section is 4.4% corresponding to cut 2 for W^- or 4% corresponding to cut 1 for W^+ , and the maximum error in the acceptance is 0.64 % or 0.46 % for the cut 2 for W^+ or W^- correspondingly.

4. NNLO QCD Uncertainties

QCD uncertainties include errors due to missing higher-order corrections in the hard matrix element, uncertainties in the parton distribution functions, and approximations made in the

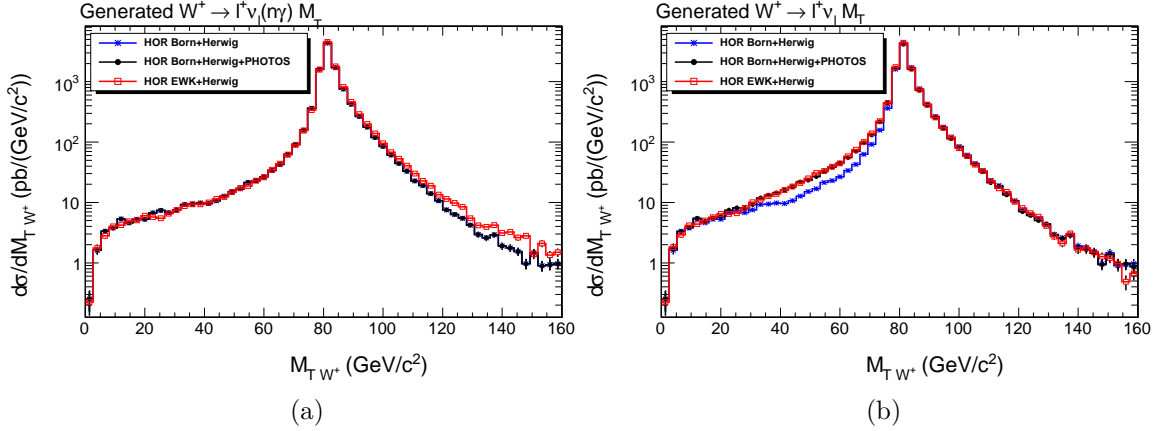


Figure 1: Comparison of the generated (a) W^+ boson transverse mass distributions and (b) $\ell^+\nu_\ell$ transverse mass distributions for the process $W^+ \rightarrow \ell^+\nu_\ell(n\gamma)$ in HORACE 3.1 including $\mathcal{O}(\alpha)$ EWK corrections showered with HERWIG (open red squares), HORACE Born-level showered with HERWIG plus PHOTOS (black circles), and HORACE Born-level (blue stars).

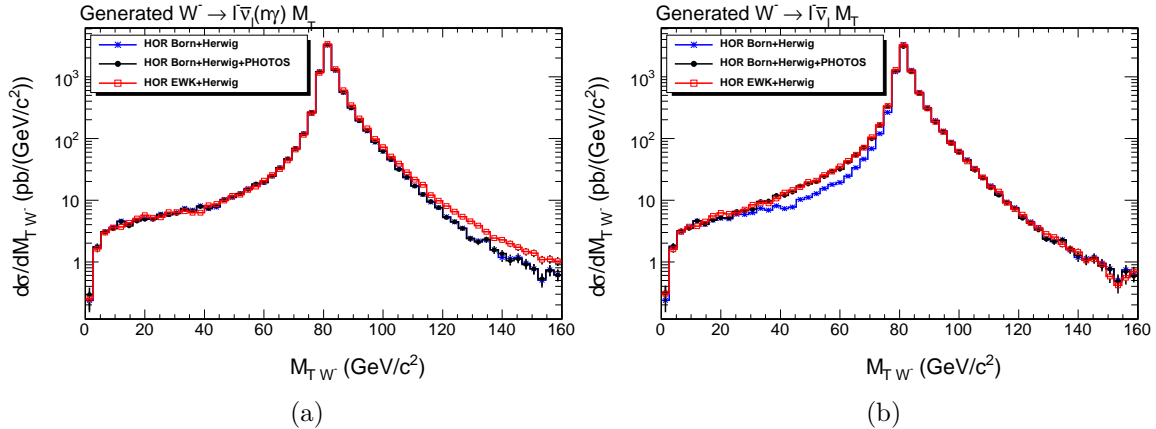


Figure 2: Comparison of the generated (a) W^- boson transverse mass distributions and (b) $\ell^-\bar{\nu}_\ell$ transverse mass distributions for the process $W^- \rightarrow \ell^-\bar{\nu}_\ell(n\gamma)$ in HORACE 3.1 including $\mathcal{O}(\alpha)$ EWK corrections showered with HERWIG (open red squares), HORACE Born-level showered with HERWIG plus PHOTOS (black circles), and HORACE Born-level (blue stars).

showering algorithms. In the following, we will evaluate the errors introduced by omitting the NNLO corrections by using MC@NLO, and calculate K -factors which can be used to introduce NNLO corrections to the MC@NLO calculation. We will also examine the effect of uncertainties in the PDFs. For these studies, we choose the same three sets of cuts as given previously in Table 1.

We begin by examining the NNLO corrections, using the state-of-the-art program FEWZ [7], which is differential in the and the lepton transverse momenta and pseudorapidities. The FEWZ program is at NNLO in perturbative QCD, includes spin correlations, and

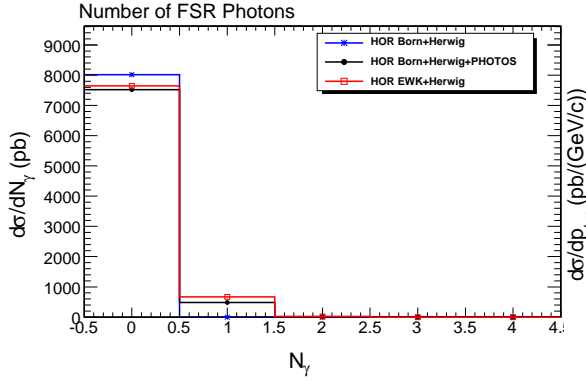


Figure 3: Comparison of the number n of hard final state radiation (FSR) photons in $W \rightarrow \ell\nu(n\gamma)$ for HORACE 3.1 including $\mathcal{O}(\alpha)$ EWK corrections showered with HERWIG (open red squares), HORACE Born-level showered with HERWIG plus PHOTOS (black circles), and HORACE Born-level (blue stars).

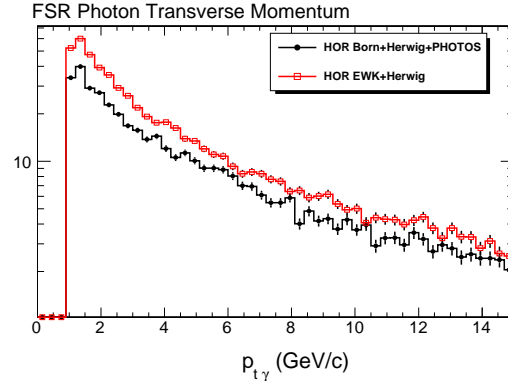


Figure 4: Comparison of $W \rightarrow \ell\nu(n\gamma)$ final state radiation (FSR) transverse momentum distributions for HORACE 3.1 including EWK corrections showered with HERWIG (open red squares) and HORACE Born-level showered with HERWIG plus PHOTOS (black circles).

takes into account finite widths effects. Since we are interested primarily in studies about the W peak, we choose the renormalization and factorization scales to be $\mu_F = \mu_R = M_W$. Scale dependence will be discussed in detail the next section.

A comparison of the effects of higher order QCD corrections on the cross-section and acceptance is presented in Tables 4 – 5 and Figs. 5 – 8. Both the NLO and NNLO calculations are done with CTEQ6.5M PDFs [22], since we will be calculating K -factors intended to rescale NLO calculations which have used these PDFs. However, since CTEQ6.5M PDFs are only available at NLO, we have also repeated the calculations in the tables using MRST PDFs, and found the results to be compatible, as will be discussed later in this

NNLO Cross Sections σ (pb) for W^+ Production

Cut	MC@NLO	FEWZ NLO	FEWZ NNLO	K -factor	$K \times \text{MC@NLO}$
σ^{tot}	12587 ± 13	12869 ± 12	12780 ± 48	0.9931 ± 0.0039	12500 ± 51
1	2072.6 ± 6.0	2157.6 ± 2.2	2122.9 ± 14.7	0.9839 ± 0.0069	2039.2 ± 15.5
2	2541.8 ± 6.5	2682.4 ± 2.7	2651.6 ± 21.2	0.9885 ± 0.0079	2512.6 ± 21.1
3	1575.0 ± 5.4	1656.0 ± 1.6	1605.8 ± 13.1	0.9970 ± 0.0080	1570.3 ± 13.7

NNLO Acceptances (%) for W^+ Production

Cut	MC@NLO	FEWZ NLO	FEWZ NNLO	K -factor	$K \times \text{MC@NLO}$
1	16.47 ± 0.05	16.77 ± 0.02	16.61 ± 0.13	0.9908 ± 0.0079	16.31 ± 0.14
2	20.19 ± 0.05	20.84 ± 0.03	20.75 ± 0.18	0.9954 ± 0.0089	20.10 ± 0.19
3	12.51 ± 0.04	12.87 ± 0.02	12.57 ± 0.11	0.9765 ± 0.0089	12.22 ± 0.12

Table 4: Calculation of the $W^+ \rightarrow \ell^+ \nu_\ell$ ($\ell = e$ or μ) cross-section at NLO using MC@NLO, and at NLO and NNLO using FEWZ, for the cut region defined in Table 1.

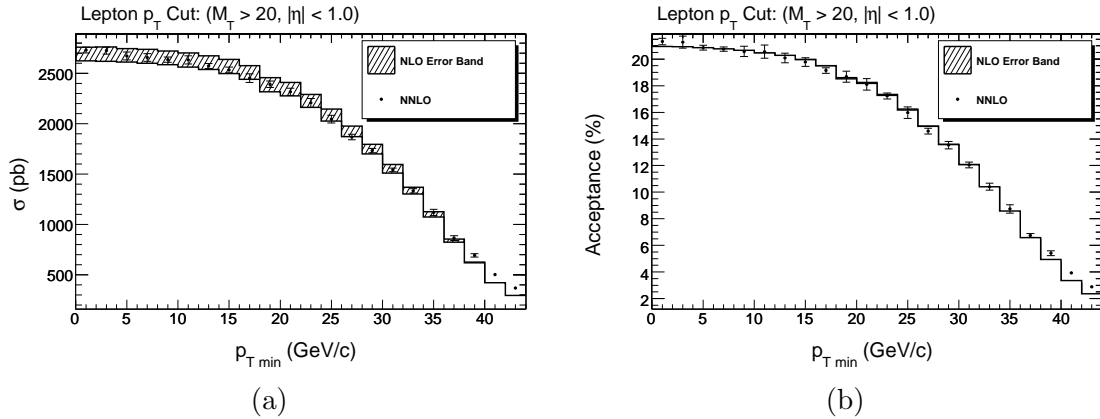


Figure 5: Cross-section (a) and acceptance (b) versus cut on lepton p_T at NLO (hashed bands) and NNLO (points), as calculated using FEWZ for $W^+ \rightarrow \ell^+ \nu_\ell$.

section. All results in the tables are calculated at scale M_W . In the figures, the NLO results are displayed as a band spanning the range of scales from $M_W/2$ to $2M_W$. The scale dependence of the NNLO result is small enough to be comparable to the precision of the MC evaluation of the integrals, so only the average of the high and low scales is plotted, with error bars reflecting a combination of statistical and scale variation uncertainties.

Since the NNLO matrix element has not yet been interfaced to a shower, we cannot directly compare FEWZ to MC@NLO. The best we can do at this time is to use MC@NLO to obtain the NLO showered result, and multiply this by a K -factor obtained by taking the ratio of the NNLO to NLO results derived from FEWZ. This procedure is reasonable except in threshold regimes where the fixed-order NLO result in FEWZ would be unreliable. This is similar to methods that have been used for calculating NNLO corrections to Higgs production [23]. The differences of these K -factors from unity are shown in Figs. 9 and 10 for both the cross-sections and acceptances, as a function of cuts on the lepton p_T and η .

NNLO Cross Sections σ (pb) for W^- Production

Cut	MC@NLO	FEWZ NLO	FEWZ NNLO	K -factor	$K \times \text{MC@NLO}$
σ^{tot}	9202.5 ± 9.9	9450.5 ± 9.2	9357.6 ± 34.7	0.9902 ± 0.0038	9112.3 ± 36.3
1	1733.5 ± 4.6	1794.0 ± 1.8	1772.1 ± 14.3	0.9878 ± 0.0080	1712.4 ± 14.6
2	1858.3 ± 4.8	1950.7 ± 1.9	1890.4 ± 21.4	0.9691 ± 0.0110	1800.9 ± 21.0
3	1341.2 ± 4.2	1404.1 ± 1.4	1355.1 ± 13.1	0.9651 ± 0.0094	1294.4 ± 13.2

NNLO Acceptances (%) for W^- Production

Cut	MC@NLO	FEWZ NLO	FEWZ NNLO	K -factor	$K \times \text{MC@NLO}$
1	18.84 ± 0.05	18.98 ± 0.03	18.94 ± 0.17	0.9976 ± 0.0090	18.79 ± 0.18
2	20.19 ± 0.05	20.64 ± 0.03	20.20 ± 0.24	0.9787 ± 0.0118	19.76 ± 0.24
3	14.58 ± 0.05	14.86 ± 0.02	14.48 ± 0.15	0.9747 ± 0.0102	14.21 ± 0.16

Table 5: Calculation of the $W^- \rightarrow \ell^- \bar{\nu}_\ell$ ($\ell = e$ or μ) cross-section at NLO using MC@NLO, and at NLO and NNLO using FEWZ, for the cut region defined in Table 1.

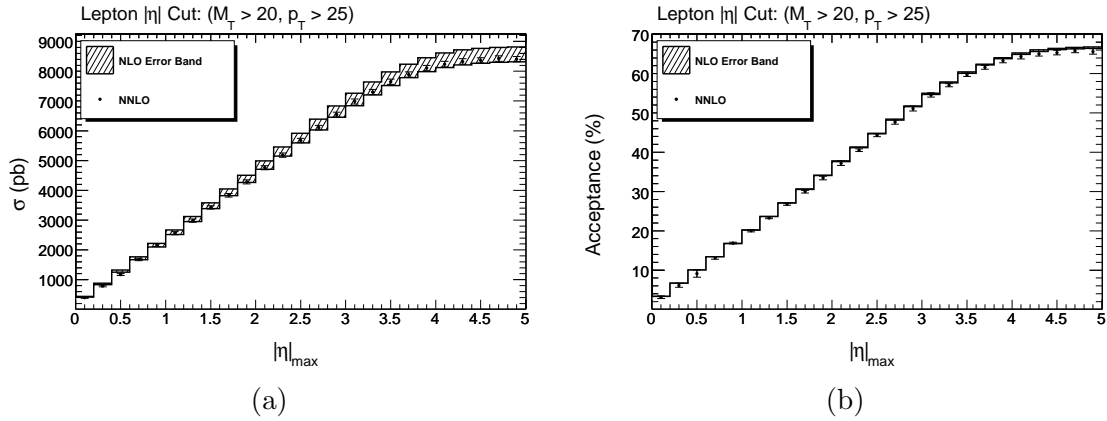


Figure 6: Cross-section (a) and acceptance (b) versus cut on lepton $|\eta|$ at NLO (hashed bands) and NNLO (points), as calculated using FEWZ for $W^+ \rightarrow \ell^+ \nu_\ell$.

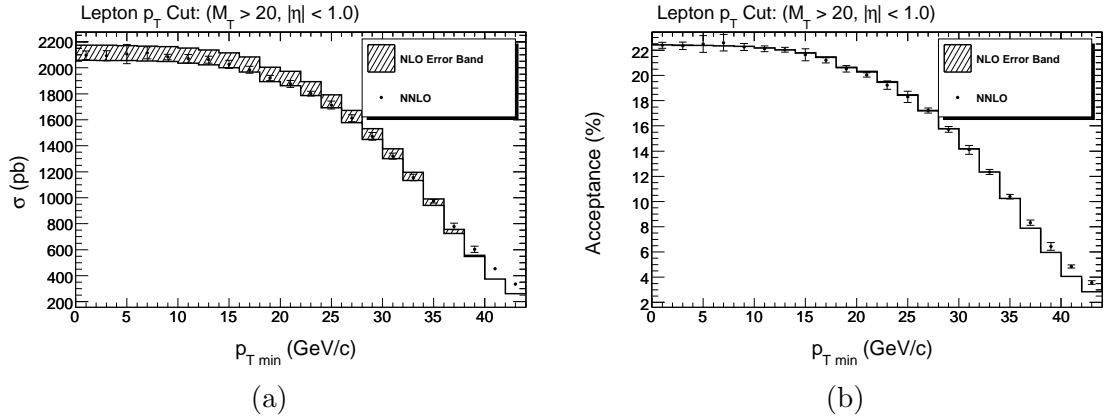


Figure 7: Cross-section (a) and acceptance (b) versus cut on lepton p_T at NLO (hashed bands) and NNLO (points), as calculated using FEWZ for $W^- \rightarrow \ell^- \bar{\nu}_\ell$.

The resulting accepted cross-section is shown in the $K \times \text{MC@NLO}$ column of Tables 4 – 5 and in Figs. 11 and 12 as a function of the same cuts as in Figs. 9 and 10. The size of $K - 1$ is a good indicator of the error due to missing NNLO if MC@NLO is used without corrections.

The results in Tables 4 – 5 show K -factors corresponding to an NNLO correction of about 1% for the W^\pm cross-sections, or up to 3.5% for the Cut 3 cross-section. NNLO corrections to the acceptances were generally at the 2.5% level or less, with Cut 3 again having the biggest corrections. Cut 1 acceptances had a 1% or less correction for both W^\pm . Convergence of the FEWZ W calculation appears better than for the Z calculation, giving more rapid convergence and smaller Monte-Carlo errors in comparable run-times. Thus, 1% evaluations were generally possible in the W calculation, but were not always practical in the corresponding Z calculations.[3]

As noted above, the CTEQ6.5M PDFs do not include NNLO corrections, it is important to check their compatibility with the NNLO calculation by repeating the calculation

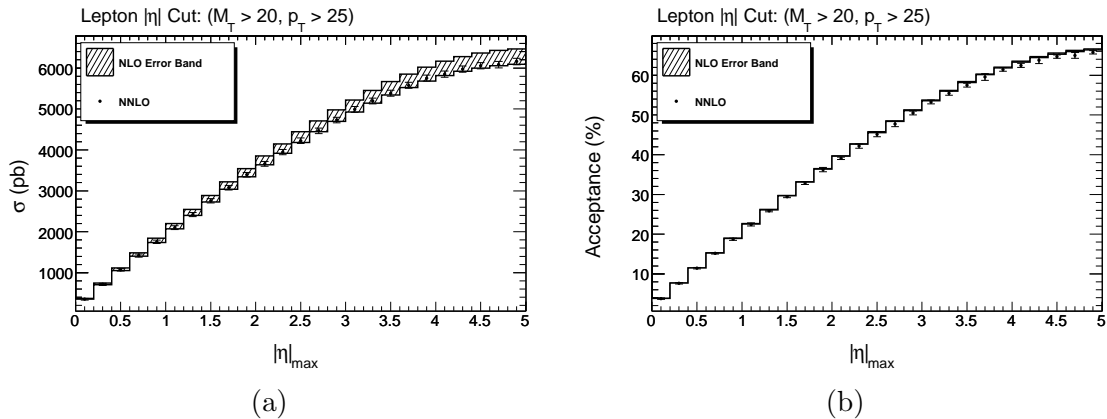


Figure 8: Cross-section (a) and acceptance (b) versus cut on lepton $|\eta|$ at NLO (hashed bands) and NNLO (points), as calculated using FEWZ for $W^- \rightarrow \ell^- \bar{\nu}_\ell$.

K-factors with CTEQ and MRST PDFs

Cut	CTEQ $K(\sigma)$	MRST $K(\sigma)$	CTEQ $K(A)$	MRST $K(A)$
W^+ cut 1	0.9839 ± 0.0069	0.9767 ± 0.0081	0.9908 ± 0.0079	0.9988 ± 0.0091
W^- cut 1	0.9878 ± 0.0080	0.9538 ± 0.0086	0.9976 ± 0.0090	0.9804 ± 0.0097
W^+ cut 2	0.9885 ± 0.0079	0.9745 ± 0.0100	0.9954 ± 0.0089	0.9966 ± 0.0110
W^- cut 2	0.9691 ± 0.0110	0.9712 ± 0.0109	0.9787 ± 0.0118	0.9984 ± 0.0119
W^+ cut 3	0.9697 ± 0.0080	0.9510 ± 0.0097	0.9765 ± 0.0089	0.9725 ± 0.0106
W^- cut 3	0.9651 ± 0.0094	0.9430 ± 0.0209	0.9747 ± 0.0102	0.9694 ± 0.0218

Table 6: Comparison of the K factors for cross-sections and acceptances calculated using CTEQ6.5M (NLO) and MRST 2002 (NNLO) PDFs for both W^+ and W^- production. $K(\sigma)$ is the K -factor for the cross-section and $K(A)$ is the K -factor for the acceptance, as displayed in Tables 4 – 5.

with MRST 2002 NNLO PDFs. It is not obvious that substituting NLO PDFs in this calculation is reasonable, but in fact, it turns out to be. The K -factors for the cross-section and acceptance for each of the three cuts is shown in Table 6 for both sets of PDFs. The $K(\sigma)$ -factors are ratios of NNLO to NLO cross-sections, and $K(A)$ are ratios of NNLO to NLO acceptances relative to the total cross section. The agreement of the K factors for the cross sections varies from less than 1% to 3.6%, with the maximum disagreement for W^- cut 1. The acceptances agree to within 1% except for W^- cuts 1 and 2, where the agreement is within 2%. There is still some variation in the results due to the slow convergence of the NNLO calculation, typically in the 1 – 2% range. Only cut 1 for the W^- has a PDF dependence outside that range, and this could still be primarily due to Monte Carlo errors.

5. Scale Dependence

Perturbative QCD calculations at fixed order depend on the factorization and renormalization scales introduced in the calculation. Thus, the previous calculations have an added

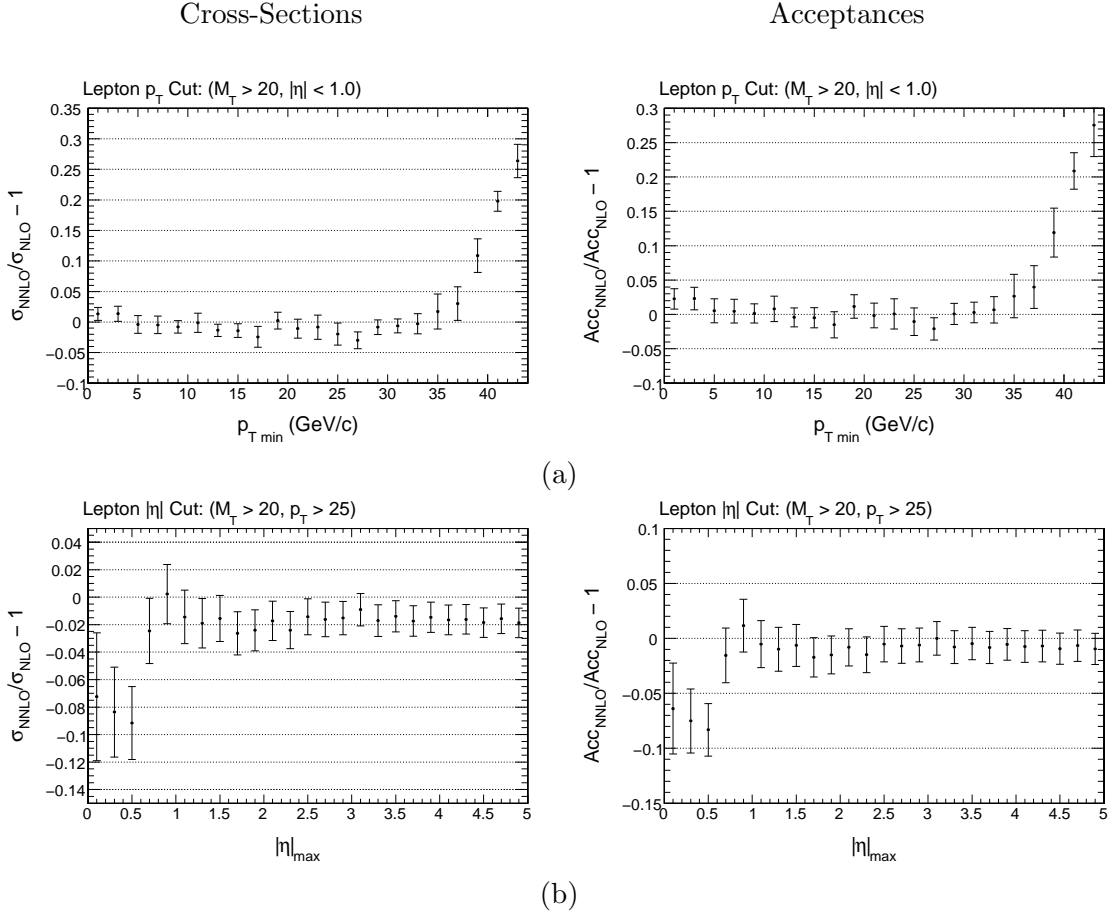


Figure 9: Fractional difference in the NNLO and NLO cross-sections (left-hand side) and acceptances (right-hand side) as a function of the lepton (a) p_T , and (b) $|\eta|$ cuts as in Figs. Figs 5 – 6 for $W^+ \rightarrow \ell^+ \nu_\ell$. These differences are the factor $K - 1$ for the cross-section and acceptances, respectively.

uncertainty due to the choice of certain fictitious scales appearing in the calculation. In a complete, all order calculation, or one completely resummed in the soft and collinear regimes and properly matched to the PDFs, there would be no dependence on these scales. However, in a fixed order calculation matched to PDFs, a dependence on the factorization scale μ_F and renormalization scale μ_R appear in the final results. The effect of scale choice is significant at NLO. Adding NNLO effects is found to reduce scale dependence considerably [6, 7], though it can remain significant near thresholds where NLO effectively becomes leading order.

As is customary, we will choose the renormalization and factorization scales to be identical, and investigate the scale dependence by varying them by a factor of 2 or 1/2 about a central value of $\mu_{F,R} = M_Z$, which is typical of the scales in our acceptance, and was the central value chosen in the previous section.

Tables 4 – 5 included only the central scale M_W . Tables 7 – 10 show the total cross sections and acceptances for lepton production calculated by FEWZ at three different

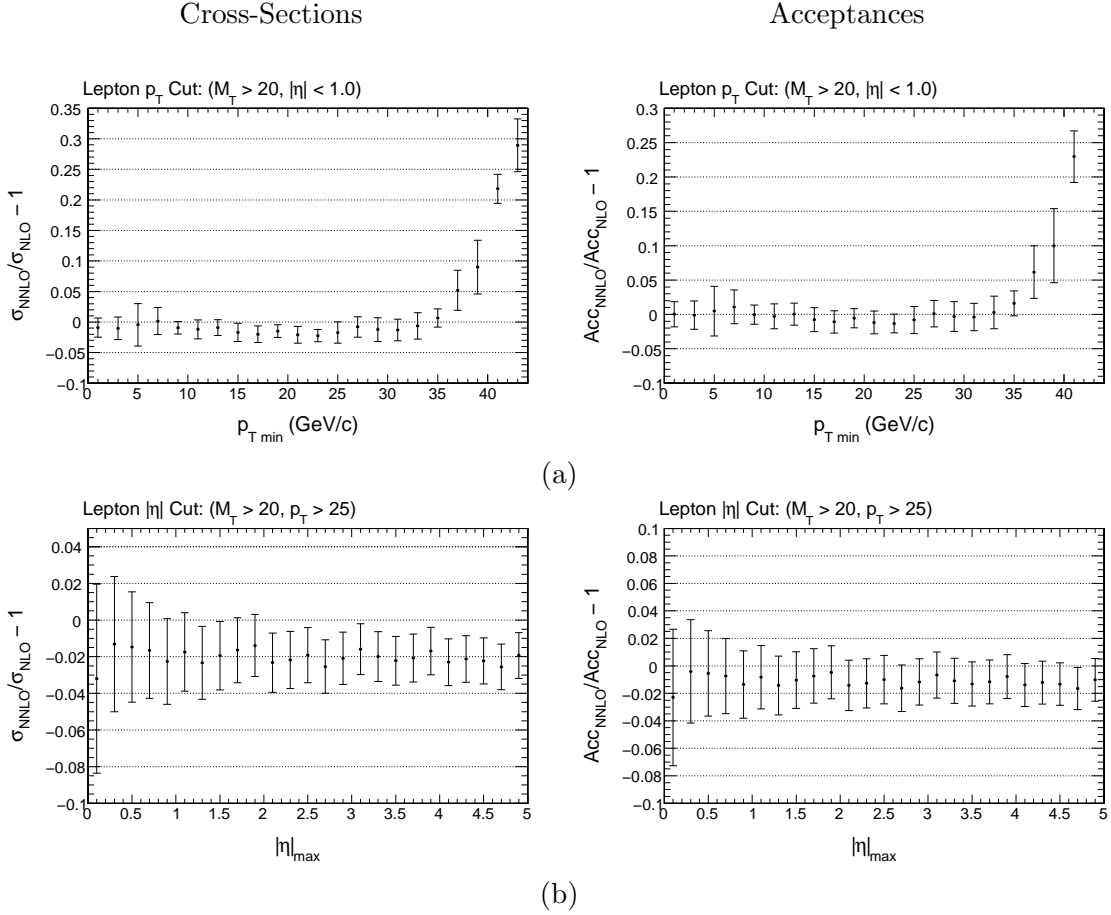


Figure 10: Fractional difference in the NNLO and NLO cross-sections (left-hand side) and acceptances (right-hand side) as a function of the lepton (a) p_T , and (b) $|\eta|$ cuts as in Figs. Figs 7 – 8 for $W^- \rightarrow \ell^- \bar{\nu}_\ell$. These differences are the factor $K - 1$ for the cross-section and acceptances, respectively.

renormalization and factorization scales $M_W/2$, M_W , and $2M_W$. The acceptances for the final state leptons are as defined in Table 1. For a measure of the size of the scale dependence, the final column of each table shows the maximum difference between the three values divided by average, with an error calculated assuming the statistical errors in the three MC runs in each row are independent.

We can see that the scale dependence of the cross-sections at NLO is typically of order $\pm 6\%$. The scale dependence of NLO acceptances is dramatically reduced due to correlations in the scale dependence of the cut and uncut cross-sections used to compute it. Adding NNLO reduces the scale dependence of the cross-sections to less than 2% in most cases. For some cuts, the convergence of the Monte-Carlo is a significant limitation on the accuracy of this result, since the NNLO MC errors can be comparable to the scale dependence.

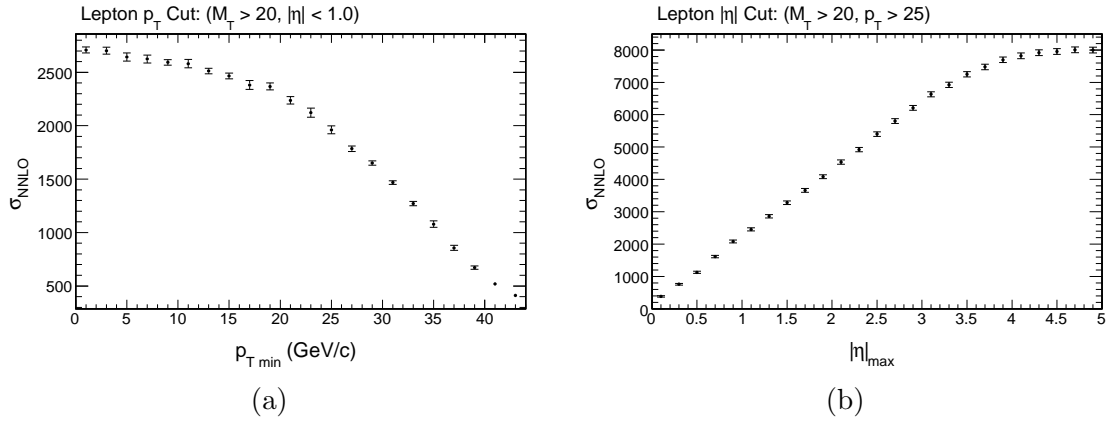


Figure 11: Accepted NNLO cross-section estimated from MC@NLO scaled by the K -factor versus the lepton (a) p_T , and (b) $|\eta|$ cuts for $W^+ \rightarrow \ell^+ \nu_\ell$.

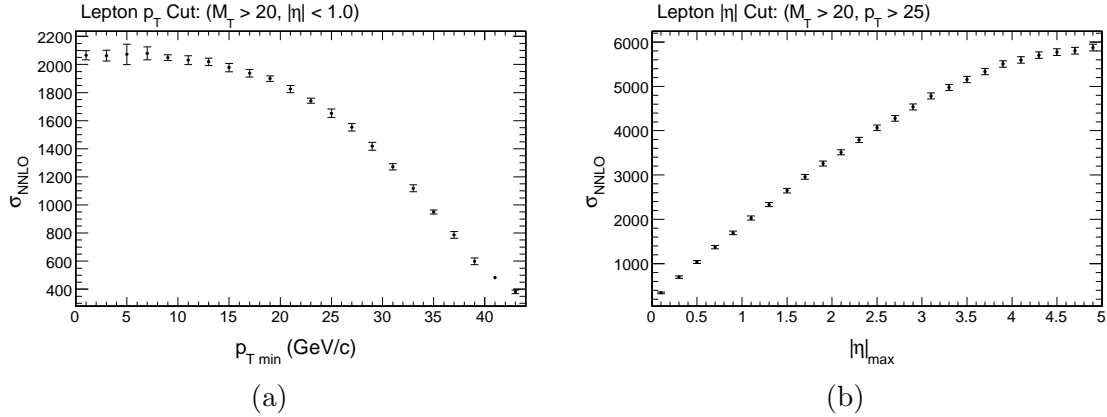


Figure 12: Accepted NNLO cross-section estimated from MC@NLO scaled by the K -factor versus the lepton (a) p_T , and (b) $|\eta|$ cuts for $W^- \rightarrow \ell^- \bar{\nu}_\ell$.

6. Uncertainties Due to the Parton Distribution Function

Phenomenological parameterizations of the PDFs are taken from a global fit to data. Therefore, uncertainties on the PDFs arising from diverse experimental and theoretical sources will propagate from the global analysis into the predictions for the W/Z cross-sections. Figure 13 and Figure 14 show the results of the inclusive W to di-lepton production cross-section using various CTEQ [22] and MRST [25] PDFs. The upward shift of about 7% (between CTEQ6.1 and 6.5 and MRST2004 and 2006) results from the inclusion of heavy quark effects in the latest PDF calculations. The acceptance due to the cuts in Table 1 using each of these PDFs is shown in Fig. 15 and Fig. 16.¹

The uncertainties in the PDFs arising from the experimental statistical and systematic uncertainties, and the effect on the production cross-section of the W boson, have been

¹Theoretical issues which may affect the contribution of the PDFs to the NNLO K -factor are not included here as we are concerned primarily with the error at NLO. See Refs. [26] for details.

Total Cross-Section (in pb): W^+

Order	$M_W/2$	M_W	$2M_W$	$\Delta\sigma/\bar{\sigma}$
NLO	12517 ± 11.6	12869 ± 11.9	13203 ± 13.2	0.0534 ± 0.0013
NNLO	12708 ± 63.6	12780 ± 48.2	12903 ± 49.7	0.0153 ± 0.0060

Cut Region 1: W^+

Order	$M_W/2$	M_W	$2M_W$	$\Delta\sigma/\bar{\sigma}$
NLO	2096.9 ± 2.1	2157.6 ± 2.2	2220.1 ± 2.2	0.0571 ± 0.0014
NNLO	2123.3 ± 23.2	2122.9 ± 14.7	2139.8 ± 15.7	0.0079 ± 0.0121

Cut Region 2: W^+

Order	$M_W/2$	M_W	$2M_W$	$\Delta\sigma/\bar{\sigma}$
NLO	2608.3 ± 2.6	2682.4 ± 2.7	2762.0 ± 2.7	0.0572 ± 0.0014
NNLO	2606.5 ± 24.6	2651.6 ± 21.2	2643.6 ± 19.5	0.0172 ± 0.0117

Cut Region 3: W^+

Order	$M_W/2$	M_W	$2M_W$	$\Delta\sigma/\bar{\sigma}$
NLO	1607.6 ± 1.6	1656.0 ± 1.6	1703.3 ± 1.7	0.0578 ± 0.0014
NNLO	1620.4 ± 11.8	1605.8 ± 13.1	1625.6 ± 13.7	0.0122 ± 0.0113

Table 7: Scale dependence of the total and accepted cross-sections (in pb) for W^+ boson production calculated by the FEWZ program at order NLO and NNLO. The final column is a measure of scale dependence obtained by dividing the maximum spread by the average for the three points.

Cut Region 1: W^+ (% Accepted)

Order	$M_W/2$	M_W	$2M_W$	$\Delta A/\bar{A}$
NLO	16.75 ± 0.02	16.77 ± 0.02	16.82 ± 0.02	0.0037 ± 0.0020
NNLO	16.71 ± 0.20	16.61 ± 0.13	16.58 ± 0.14	0.0076 ± 0.0136

Cut Region 2: W^+ (% Accepted)

Order	$M_W/2$	M_W	$2M_W$	$\Delta A/\bar{A}$
NLO	20.84 ± 0.03	20.84 ± 0.03	20.92 ± 0.03	0.0039 ± 0.0020
NNLO	20.51 ± 0.22	20.75 ± 0.18	20.49 ± 0.17	0.0127 ± 0.0132

Cut Region 3: W^+ (% Accepted)

Order	$M_W/2$	M_W	$2M_W$	$\Delta A/\bar{A}$
NLO	12.84 ± 0.02	12.87 ± 0.02	12.90 ± 0.02	0.0045 ± 0.0020
NNLO	12.75 ± 0.11	12.57 ± 0.11	12.60 ± 0.12	0.0147 ± 0.0128

Table 8: Scale dependence of the acceptances A in the various cut regions for W^+ boson production calculated by the FEWZ program at order NLO and NNLO. The final column is a measure of scale dependence obtained by dividing the maximum spread of the three preceding columns by their average.

studied using the standard methods proposed in Refs. [22, 25]. For the standard set of PDFs, corresponding to the minimum in the PDF parameter space, a complete set of eigenvector PDF sets, which characterize the region nearby the minimum and quantify its error, have been simultaneously calculated. From the minimum set and these “error” sets we calculate the best estimate and the uncertainty for the W cross-section. We do this

Total Cross-Section (in pb): W^-

Order	$M_W/2$	M_W	$2M_W$	$\Delta\sigma/\bar{\sigma}$
NLO	9184.6 ± 9.1	9450.5 ± 9.2	9706.5 ± 9.5	0.0553 ± 0.0014
NNLO	9307.3 ± 34.3	9357.6 ± 34.7	9419.5 ± 36.0	0.0120 ± 0.0053

Cut Region 1: W^-

Order	$M_W/2$	M_W	$2M_W$	$\Delta\sigma/\bar{\sigma}$
NLO	1741.4 ± 1.7	1794.0 ± 1.8	1842.4 ± 1.8	0.0563 ± 0.0014
NNLO	1717.5 ± 13.5	1772.1 ± 14.3	1767.8 ± 12.6	0.0312 ± 0.0109

Cut Region 2: W^-

Order	$M_W/2$	M_W	$2M_W$	$\Delta\sigma/\bar{\sigma}$
NLO	1894.0 ± 1.9	1950.7 ± 1.9	2005.5 ± 2.0	0.0572 ± 0.0014
NNLO	1892.9 ± 15.7	1890.4 ± 21.4	1906.4 ± 15.0	0.0084 ± 0.0131

Cut Region 3: W^-

Order	$M_W/2$	M_W	$2M_W$	$\Delta\sigma/\bar{\sigma}$
NLO	1360.2 ± 1.4	1404.1 ± 1.4	1449.3 ± 1.5	0.0634 ± 0.0014
NNLO	1343.8 ± 11.8	1355.1 ± 13.1	1358.7 ± 13.7	0.0110 ± 0.0135

Table 9: Scale dependence of the total and accepted cross-sections (in pb) for W^- boson production calculated by the FEWZ program at order NLO and NNLO. The final column is a measure of scale dependence obtained by dividing the maximum spread by the average for the three points.

Cut Region 1: W^- (% Accepted)

Order	$M_W/2$	M_W	$2M_W$	$\Delta A/\bar{A}$
NLO	18.96 ± 0.03	18.98 ± 0.03	18.98 ± 0.03	0.0013 ± 0.0020
NNLO	18.45 ± 0.16	18.94 ± 0.17	18.77 ± 0.15	0.0259 ± 0.0121

Cut Region 2: W^+ (% Accepted)

Order	$M_W/2$	M_W	$2M_W$	$\Delta A/\bar{A}$
NLO	20.62 ± 0.03	20.64 ± 0.03	20.66 ± 0.03	0.0019 ± 0.0020
NNLO	20.34 ± 0.18	20.20 ± 0.24	20.24 ± 0.18	0.0067 ± 0.0142

Cut Region 3: W^+ (% Accepted)

Order	$M_W/2$	M_W	$2M_W$	$\Delta A/\bar{A}$
NLO	14.81 ± 0.02	14.86 ± 0.02	14.93 ± 0.02	0.0082 ± 0.0020
NNLO	14.44 ± 0.14	14.48 ± 0.15	14.42 ± 0.16	0.0039 ± 0.0145

Table 10: Scale dependence of the acceptances A in the various cut regions for W^- boson production calculated by the FEWZ program at order NLO and NNLO. The final column is a measure of scale dependence obtained by dividing the maximum spread of the three preceding columns by their average.

using the Hessian error method, where the cross-section results from the various eigenvector PDF sets have been combined according to the prescriptions found in [22]. Fig. 13 and Fig. 14 list the results for the different PDFs and Table 11 summarizes the results of the latest CTEQ and MRST PDF sets. The difference in the uncertainties (approximately a factor of two) between the results obtained from the CTEQ and MRST PDF error sets is

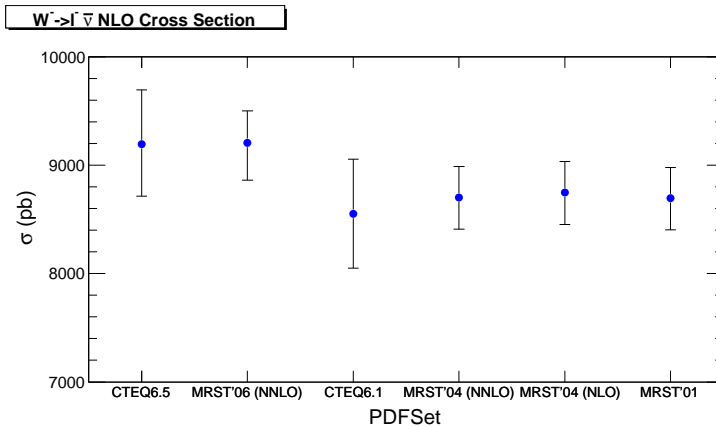


Figure 13: Comparison of $W^- \rightarrow l^- \bar{\nu}$ total cross-sections for several recent PDF calculations.

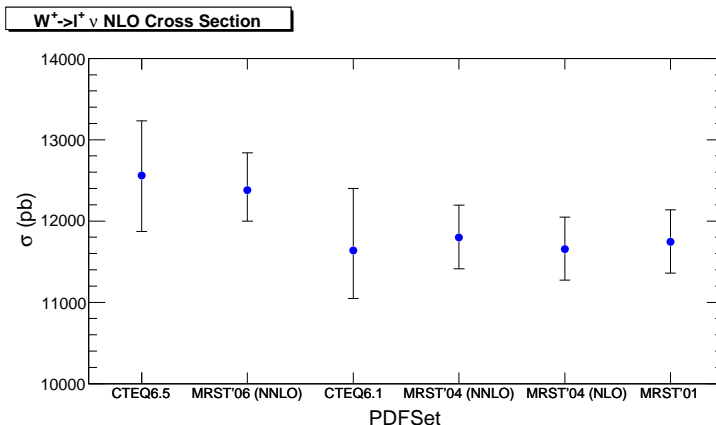


Figure 14: Comparison of $W^+ \rightarrow l^+ \nu$ total cross-sections for several recent PDF calculations.

due to different assumptions made by the groups while creating the eigenvector PDF sets.

Finally we study the sensitivity of the kinematic acceptance calculations to the uncertainties affecting the PDF sets. Figs. 17–19 for W^- and Figs. 18–20 for W^+ show the systematic error on the production cross-sections as a function of the $|\eta|$ cut and minimum lepton p_T for variations on the three types of cuts in Table 1. The fractional uncertainties, shown in the same figures, demonstrate that the relative uncertainty in the cross-section is very flat as a function of the kinematic cuts, until the region of extreme cuts and low statistics in the MC are reached. The corresponding uncertainty on the acceptance as a function of the kinematic cuts is shown in Figs 21 and 23 for W^- and Figs 22 and 24 for W^+ . These show a similar dependence to the cross-section uncertainties, though the fractional errors are smaller.

7. Conclusions

To evaluate the overall contribution from theoretical uncertainties to both the cross-section

and acceptance calculations for the decay mode $W^\pm \rightarrow \ell^\pm \nu_\ell$ ($\ell = e$ or μ) at the LHC we add the uncertainties from each of the sources considered in the preceding sections. We compile the errors assuming that the calculation is done with MC@NLO at scale $\mu_F = \mu_R = M_W$ and interfaced to PHOTOS to add final state QED radiation. The missing electroweak contribution may then be inferred from HORACE as in Sec. 3. For these errors we take those resulting from the tight cut set in Tables 2 – 3; The cuts described in Table 1 are considered the most representative of likely analysis cuts for the LHC experiments.

QCD uncertainties may be divided into two main classes. If the NNLO K -factor is set to 1, there is a missing NNLO contribution $\delta_{\text{NNLO}} = K - 1$. Since K has residual NNLO scale dependence, we must also take this into account and write $K = 1 + \delta_{\text{NNLO}} \pm \delta_{\text{scale}}$. The factor δ_{NNLO} can be inferred from Tables 4 – 5 and δ_{scale} can be inferred from half the scale variation of the NNLO entries in Tables 7 – 9, as discussed in detail in the conclusions of Ref. [3].

Both classes of QCD errors are also associated with a “technical precision” due to limitations of the computing tools used to evaluate them. Significant improvements in the NNLO precision could be obtained if a program with faster convergence were available. We therefore include an “error on the error” for the QCD errors, and propagate these through in the usual fashion to derive a final accuracy for the total QCD uncertainty estimate. This sets a limitation on how much the NLO calculation can realistically be improved using currently available NNLO results.

These contributions to QCD errors are summarized in Table 12 for the total cross-section and the three cuts of Table 1. Results are shown both for the three cut cross-sections and their ratio for the total cross-section, and the errors are assumed to be uncorrelated.

If the K -factor had not been calculated at NNLO, the error of the NLO cross-sections could have been roughly estimated from half the width of the scale-dependence band, or half the NLO results for $\Delta\sigma/\sigma$ in Tables 7 and 9, giving uncertainties of 2.8 – 3.2%. The errors calculated from the K factors are in within the limits these expectations, up to the technical precision of the calculation. A similar error NLO estimate for the error in the acceptance based on Tables 8 and 10 would predict at most 0.4% missing NNLO.

The final contribution to the total error considered here is the uncertainty from the PDFs. This may be extracted from the results of Sec. 6 by taking the errors from the CTEQ6.5 results for Cut 1 (see Table 1). The errors are asymmetric, so we take the largest of the two (up or down) uncertainties as the total fractional error for the PDF calculation. We choose the first cut set, since it is the most representative of likely analysis cuts at the LHC experiments. CTEQ errors, rather than the MRST errors, are used because they give a more conservative estimate. The difference between the results obtained by the latest CTEQ and MRST PDFs is less than the maximum error quoted for CTEQ for all three cut regions.

The errors are added in quadrature, assuming no correlations, and the results are given in Table 13. There is, in fact, no consensus on the best way to combine these errors, so the total error should be considered an estimate. The QCD error is taken for Cut 1 for the same reasons as given above. In addition, as we have discussed above, we propagate the “error on the error” for each of the contributions in order to have some reasonable estimate

of the accuracy of the quoted total theoretical uncertainty. The exception to this is the PDF error, which can be considered as an upper limit on the uncertainty, and therefore does not need an additional accuracy. We conclude that the event generator MC@NLO interfaced to PHOTOS should be sufficient to guarantee an overall theoretical uncertainty on the W production due to higher order calculation, PDFs, and renormalization scale at the level of 5.5 – 5.9% for the total cross-section of W^\mp and at approximately 2.5% for the acceptance of W^\mp .

W production will provide a valuable tool for studying QCD, measuring precision electroweak physics, and monitoring the luminosity. As the luminosity increases, the large statistics will permit a further improvement in the systematic uncertainties due to the PDFs. Adding complete $O(\alpha)$ EWK corrections to the event generator would eliminate most of the EWK uncertainty, and incorporating NNLO QCD corrections would substantially reduce the QCD uncertainties.

Reaching a combined precision of 1%, as desired in the later stages of analysis at high integrated luminosity, will require new tools. In addition to improved PDFs, an event generator combining NNLO QCD with complete $O(\alpha)$ EWK corrections will be needed, with exponentiation in appropriate regimes, and adequate convergence properties to technically reach the required precision.[27] Measurement strategies have been proposed that may mitigate some of the effects of systematic errors on the precision of the W measurements.[2] A combination of improved calculations and improved measurements will be needed to permit the desired precision to be reached as the integrated luminosity increases to a point where it is needed.

Acknowledgments

This work was supported in part by US DOE grant DE-FG02-91ER40671. We thank Frank Petriello, Zbigniew Was, Carlo M. Carloni Calame, C.-P. Yuan, and F. Piccinini for helpful correspondence. S.Y. thanks the Princeton University Department of Physics for hospitality during the completion of this work, and the 6th Simons Workshop on Mathematics and Physics at SUNY, Stony Brook for for hospitality during the preparation of the manuscript.

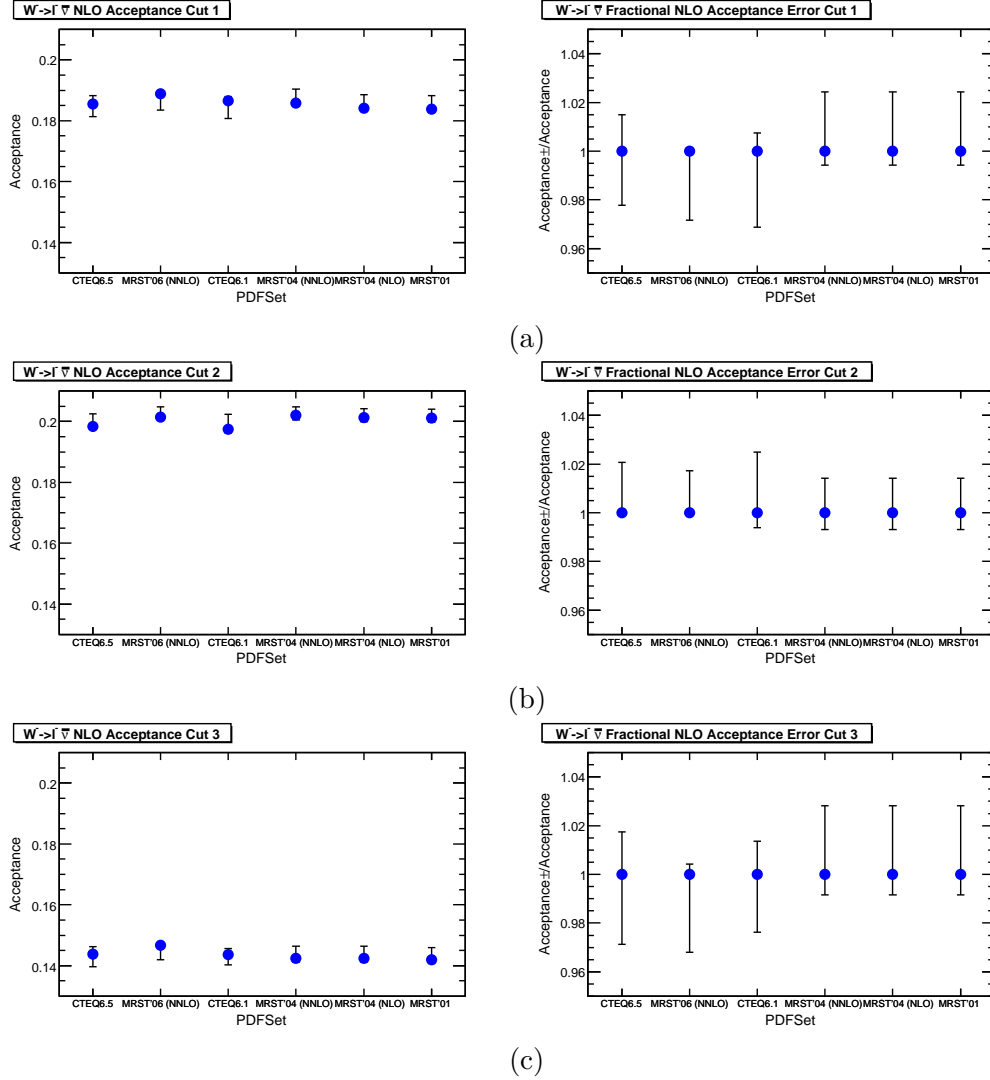


Figure 15: Comparison of $W^- \rightarrow l^- \bar{\nu}$ ($l = e$ or μ) acceptances A , with several recent PDF calculations for acceptance regions (a) Cut 1, (b) Cut 2, and (c) Cut 3, as defined in Table 1. The left-hand plots show the total acceptance and the right hand plots show the fractional error on the acceptance.

	W^-									W^+								
	No cut			Cut Region 1						No cut			Cut Region 1					
PDF Set	σ (pb)	$\Delta\sigma_+$	$\Delta\sigma_-$	σ (pb)	$\Delta\sigma_+$	$\Delta\sigma_-$	A	ΔA_+	ΔA_-	σ (pb)	$\Delta\sigma_+$	$\Delta\sigma_-$	σ (pb)	$\Delta\sigma_+$	$\Delta\sigma_-$	A	ΔA_+	ΔA_-
CTEQ6.5	9195	501	482	1787.3	57.5	59.1	0.185	0.0028	0.0041	12560	672	691	2107.26	84.4	83.5	0.158	0.0033	0.0036
MRST2006	9206	294	344	1824.2	15.0	67.0	0.189	0.0027	0.0054	12379	459	380	2106.42	23.7	45.9	0.160	0.0010	0.0031
CTEQ6.1	8552	504	503	1671.1	64.6	98.9	0.187	0.0014	0.0058	11637	763	589	1944.12	115.6	61.4	0.157	0.0047	0.0028
MRST2004 (NNLO)	8702	284	292	1681.8	48.4	22.7	0.184	0.0045	0.0011	11798	397	386	1983.64	56.9	26.5	0.159	0.0028	0.0024
MRST2004 (NLO)	8747	286	294	1703.3	49.1	23.0	0.186	0.0045	0.0011	11655	392	382	1949.68	56.0	26.1	0.157	0.0028	0.0024
MRST2001	8695	284	292	1676.7	48.3	22.6	0.184	0.0045	0.0011	11743	395	385	1937.29	55.6	25.9	0.156	0.0028	0.0024
	No cut			Cut Region 2						No cut			Cut Region 2					
	PDF Set	σ (pb)	$\Delta\sigma_+$	$\Delta\sigma_-$	σ (pb)	$\Delta\sigma_+$	$\Delta\sigma_-$	A	ΔA_+	ΔA_-	σ (pb)	$\Delta\sigma_+$	$\Delta\sigma_-$	σ (pb)	$\Delta\sigma_+$	$\Delta\sigma_-$	A	ΔA_+
CTEQ6.5	9195	501	482	1907.6	90.2	64.5	0.198	0.0041	0.0002	12560	672	691	2586.6	81.1	95.2	0.193	0.0018	0.0026
MRST2006	9206	294	344	1938.3	38.1	19.4	0.201	0.0035	0.0001	12379	459	380	2568.4	65.4	13.8	0.195	0.0033	0.0016
CTEQ6.1	8552	504	503	1767.4	95.6	64.2	0.197	0.0049	0.0012	11637	763	589	2379.47	120.9	75.9	0.192	0.0023	0.0039
MRST2004 (NNLO)	8702	284	292	1835.2	32.9	31.6	0.202	0.0028	0.0014	11798	397	386	2452.37	49.3	20.8	0.195	0.0019	0.0015
MRST2004 (NLO)	8747	286	294	1846.6	33.1	31.8	0.201	0.0028	0.0014	11655	392	382	2420.16	48.6	20.5	0.195	0.0019	0.0015
MRST2001	8695	284	292	1831.9	32.8	31.5	0.201	0.0028	0.0014	11743	395	385	2418.73	48.6	20.5	0.194	0.0019	0.0015
	No cut			Cut Region 3						No cut			Cut Region 3					
	PDF Set	σ (pb)	$\Delta\sigma_+$	$\Delta\sigma_-$	σ (pb)	$\Delta\sigma_+$	$\Delta\sigma_-$	A	ΔA_+	ΔA_-	σ (pb)	$\Delta\sigma_+$	$\Delta\sigma_-$	σ (pb)	$\Delta\sigma_+$	$\Delta\sigma_-$	A	ΔA_+
CTEQ6.5	9195	501	482	1362.5	41.9	51.8	0.144	0.0025	0.0041	12560	672	691	1572.78	73.0	64.4	0.120	0.0031	0.0030
MRST2006	9206	294	344	1392.4	15.8	56.0	0.147	0.0006	0.0047	12379	459	380	1572.68	25.6	37.8	0.122	0.0007	0.0027
CTEQ6.1	8552	504	503	1265.6	65.5	62.5	0.144	0.0019	0.0034	11637	763	589	1451.63	89.5	43.9	0.120	0.0040	0.0022
MRST2004(NNLO)	8702	284	292	1279.6	44.7	15.1	0.142	0.0040	0.0012	11798	397	386	1476.94	32.5	33.2	0.121	0.0015	0.0031
MRST2004 (NLO)	8747	286	294	1294.7	45.3	15.3	0.144	0.0041	0.0012	11655	392	382	1451.63	31.9	32.6	0.120	0.0015	0.0031
MRST2001	8695	284	292	1273.1	44.5	15.0	0.144	0.0041	0.0012	11743	395	385	1452.54	32.0	32.7	0.119	0.0015	0.0031

Table 11: Cross-sections σ for W^- and W^+ , and acceptances A , with asymmetric Hessian uncertainties as calculated using several recent PDF sets for the three cut regions defined in Table 1.

QCD Uncertainties (%)				
W^+ Cross-Section $\Delta\sigma$				
Uncertainty	σ^{tot}	Cut 1	Cut 2	Cut 3
Missing NNLO	-0.69 ± 0.39	-1.61 ± 0.69	-1.15 ± 0.79	-3.03 ± 0.80
Scale Dependence	0.76 ± 0.30	0.40 ± 0.61	0.86 ± 0.59	0.61 ± 0.56
Total	1.03 ± 0.34	1.66 ± 0.69	1.43 ± 0.73	3.09 ± 0.79
Error in W^+ Acceptance (ΔA)				
Uncertainty	–	Cut 1	Cut 2	Cut 3
Missing NNLO	–	-0.92 ± 0.79	-0.46 ± 0.89	-2.35 ± 0.89
Scale Dependence	–	0.38 ± 0.68	0.63 ± 0.66	0.74 ± 0.64
Total	–	1.00 ± 0.78	0.78 ± 0.75	2.47 ± 0.87
W^- Cross-Section $\Delta\sigma$				
Uncertainty	σ^{tot}	Cut 1	Cut 2	Cut 3
Missing NNLO	-0.98 ± 0.38	-1.22 ± 0.80	-3.09 ± 1.10	-3.49 ± 0.94
Scale Dependence	0.60 ± 0.26	1.56 ± 0.54	0.42 ± 0.66	0.55 ± 0.68
Total	1.15 ± 0.35	1.98 ± 0.65	3.12 ± 1.10	3.53 ± 0.93
Error in W^+ Acceptance (ΔA)				
Uncertainty	–	Cut 1	Cut 2	Cut 3
Missing NNLO	–	-0.24 ± 0.90	-2.13 ± 1.18	-2.53 ± 1.02
Scale Dependence	–	1.29 ± 0.61	0.34 ± 0.71	0.20 ± 0.73
Total	–	1.32 ± 0.62	2.15 ± 1.17	2.54 ± 1.02

Table 12: Summary of QCD uncertainties $\Delta\sigma$ in the cross-sections and ΔA in the acceptances relative to the un-cut cross-section σ^{tot} . The three cuts are described in Table 1. Missing NNLO is shown with a sign, because it has been calculated.

Total Theoretical Uncertainty (%)				
Uncertainty	W^-		W^+	
	Cross-Section $\Delta\sigma$	Acceptance ΔA	Cross-Section $\Delta\sigma$	Acceptance ΔA
Missing $O(\alpha)$ EWK	3.91 ± 0.57	0.05 ± 0.54	4.00 ± 0.61	0.09 ± 0.59
Total QCD	1.98 ± 0.65	1.32 ± 0.62	1.66 ± 0.69	1.00 ± 0.78
PDF	3.31	2.22	4.01	2.28
Total	5.49 ± 0.47	2.58 ± 0.32	5.90 ± 0.46	2.49 ± 0.31

Table 13: Total theoretical uncertainty on the W production cross-section $\Delta\sigma$, and acceptances ΔA .

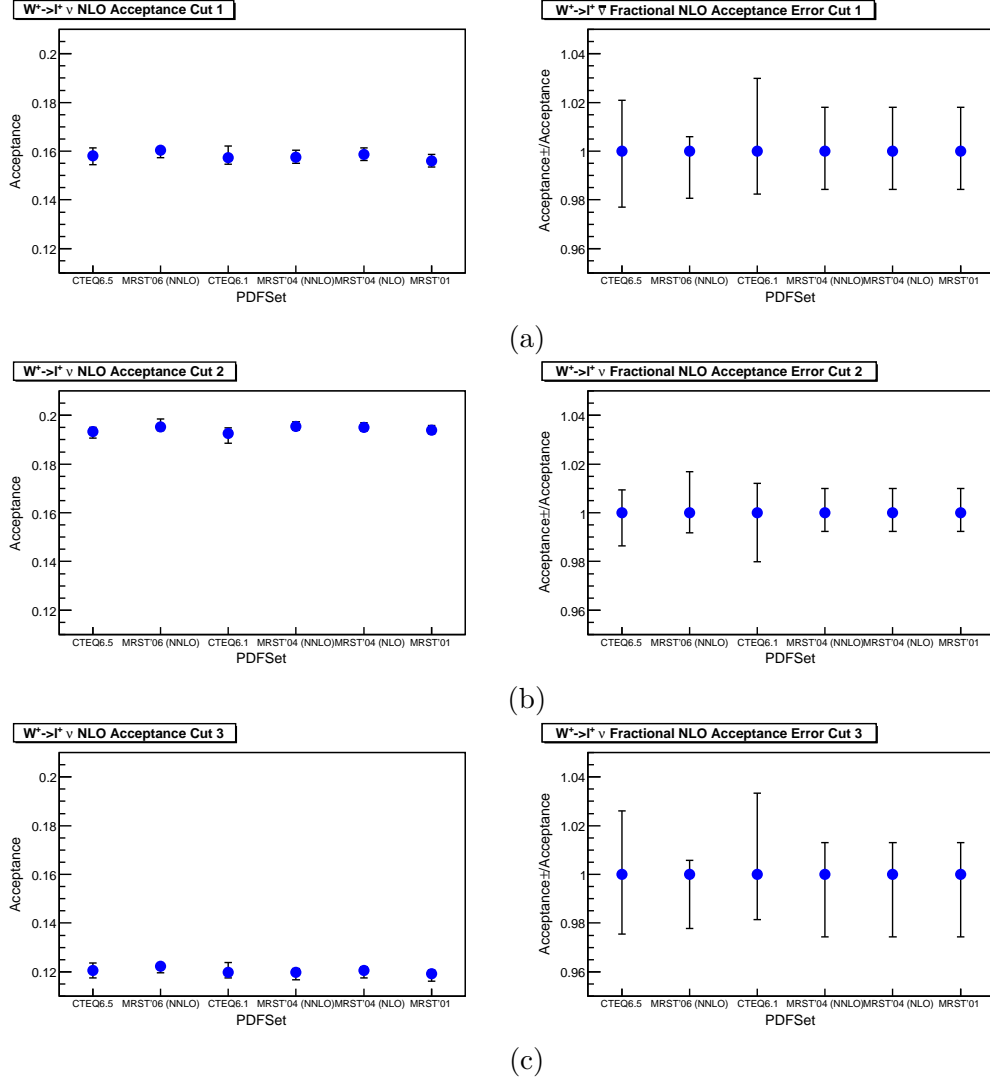


Figure 16: Comparison of $W^+ \rightarrow l^+ \nu$ ($l = e$ or μ) acceptances A , with several recent PDF calculations for acceptance regions (a) Cut 1, (b) Cut 2, and (c) Cut 3, as defined in Table 1. The left-hand plots show the total acceptance and the right hand plots show the fractional error on the acceptance.

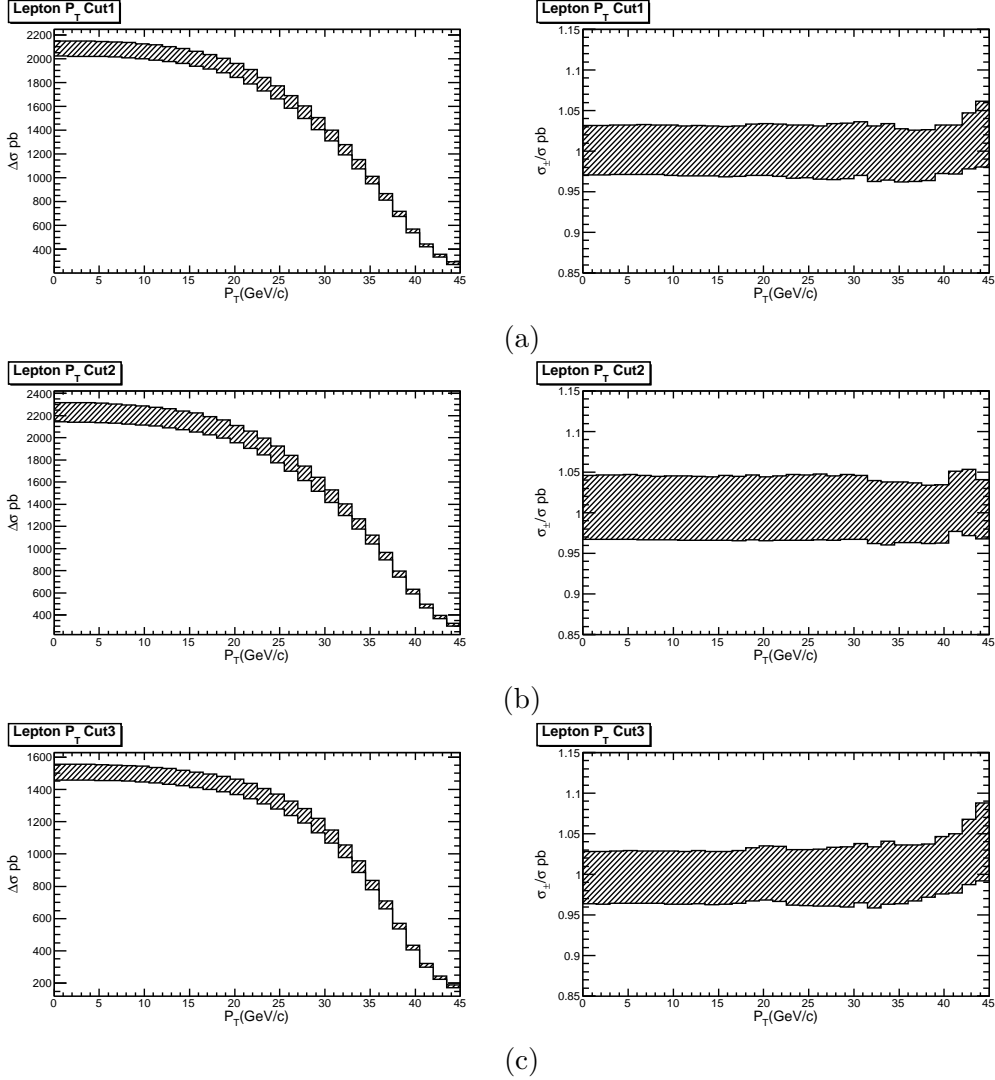


Figure 17: The $W^- \rightarrow l^- \bar{\nu}$ cross-section σ ($l = e$ or μ), as a function of the p_T cut for acceptance regions (a) Cut 1, (b) Cut 2, and (c) Cut 3, as defined in Table 1. For each acceptance region we fix the invariant mass and $|\eta|$ cuts at their specified values, and vary only the p_T cut. The figures on the right show the relative errors in the cross sections.

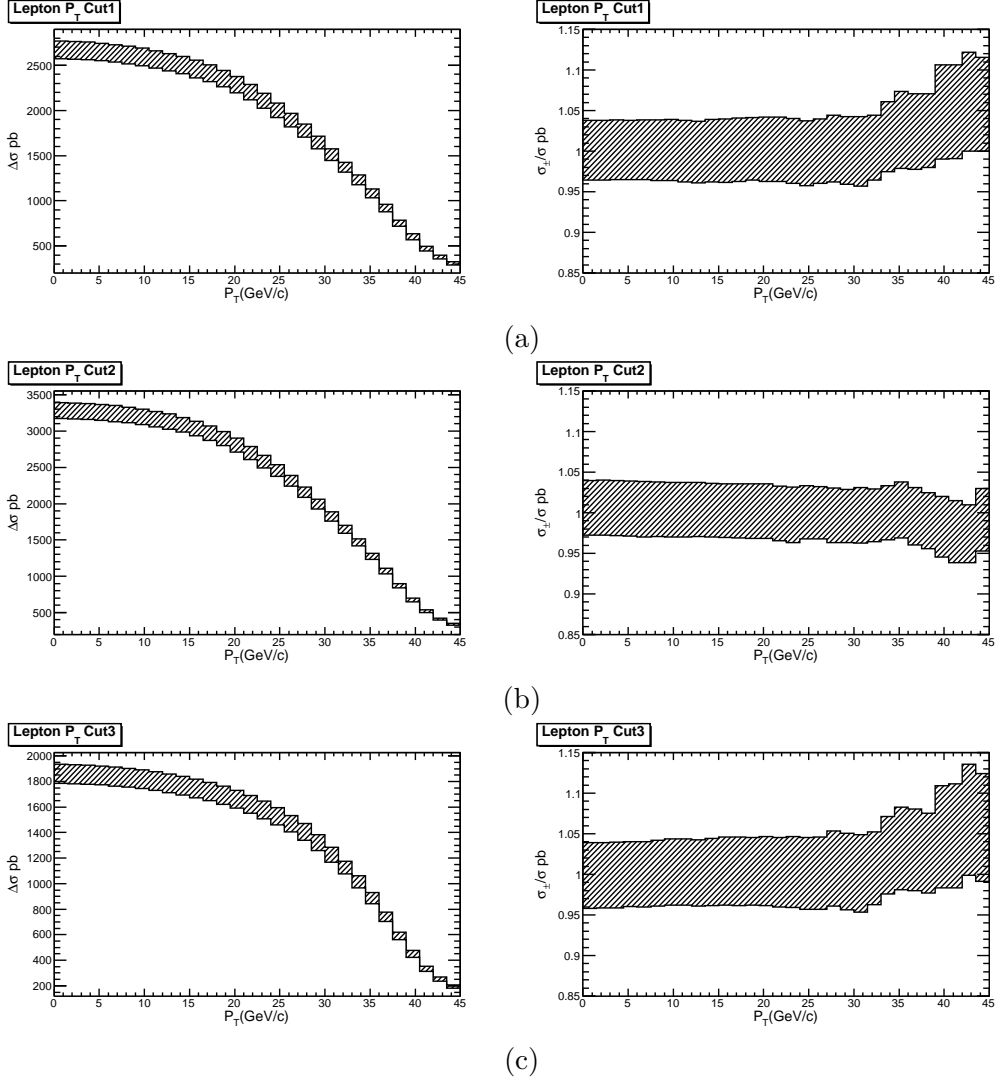


Figure 18: The $W^+ \rightarrow l^+\nu$ cross-section σ ($\ell = e$ or μ), as a function of the p_T cut for acceptance regions (a) Cut 1, (b) Cut 2, and (c) Cut 3, as defined in Table 1. For each acceptance region we fix the invariant mass and $|\eta|$ cuts at their specified values, and vary only the p_T cut. The figures on the right show the relative errors in the cross sections.

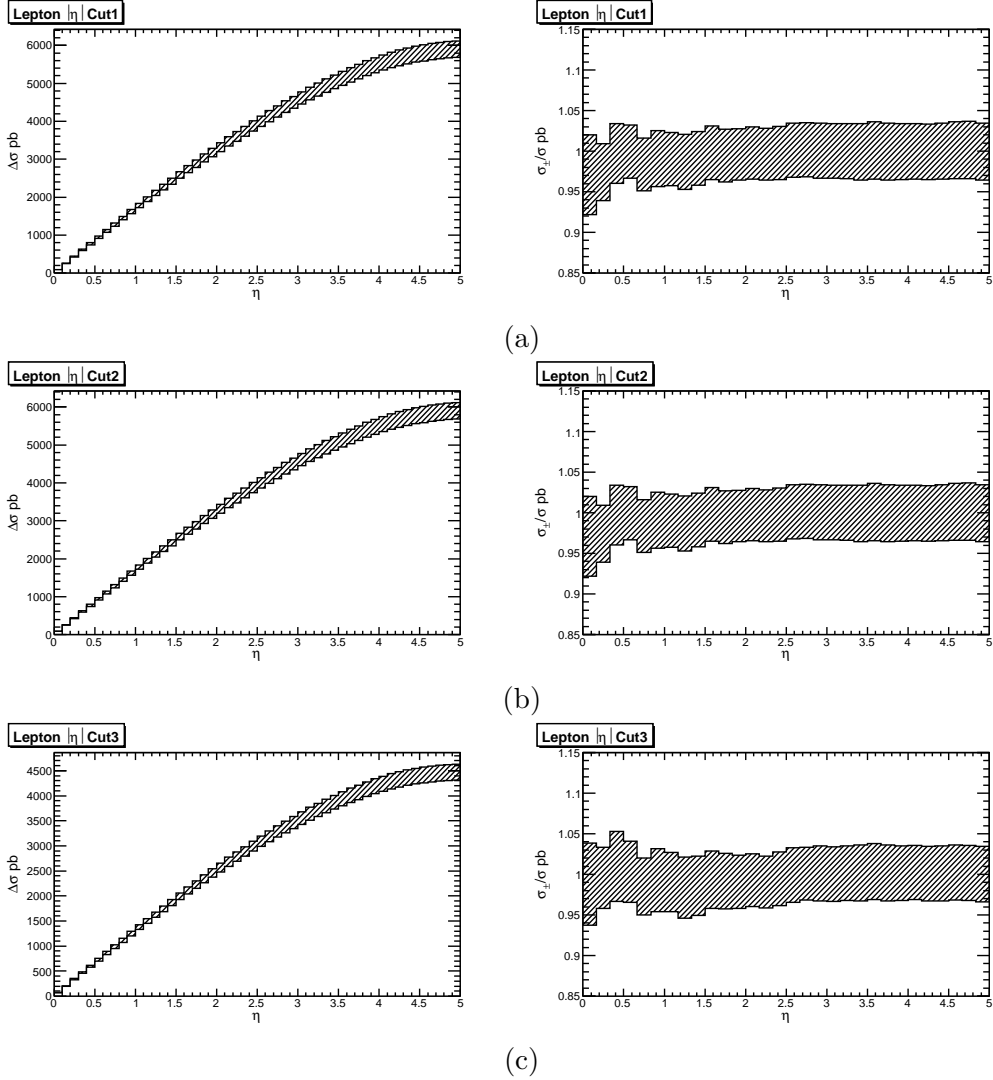


Figure 19: The $W^- \rightarrow l^- \bar{\nu}$ cross-section σ ($l = e$ or μ), as a function of the $|\eta|$ cut for acceptance regions (a) Cut 1, (b) Cut 2, and (c) Cut 3, as defined in Table 1. For each acceptance region we fix the invariant mass and p_T cuts at their specified values, and vary only the $|\eta|$ cut. The figures on the right show the relative errors in the cross sections.

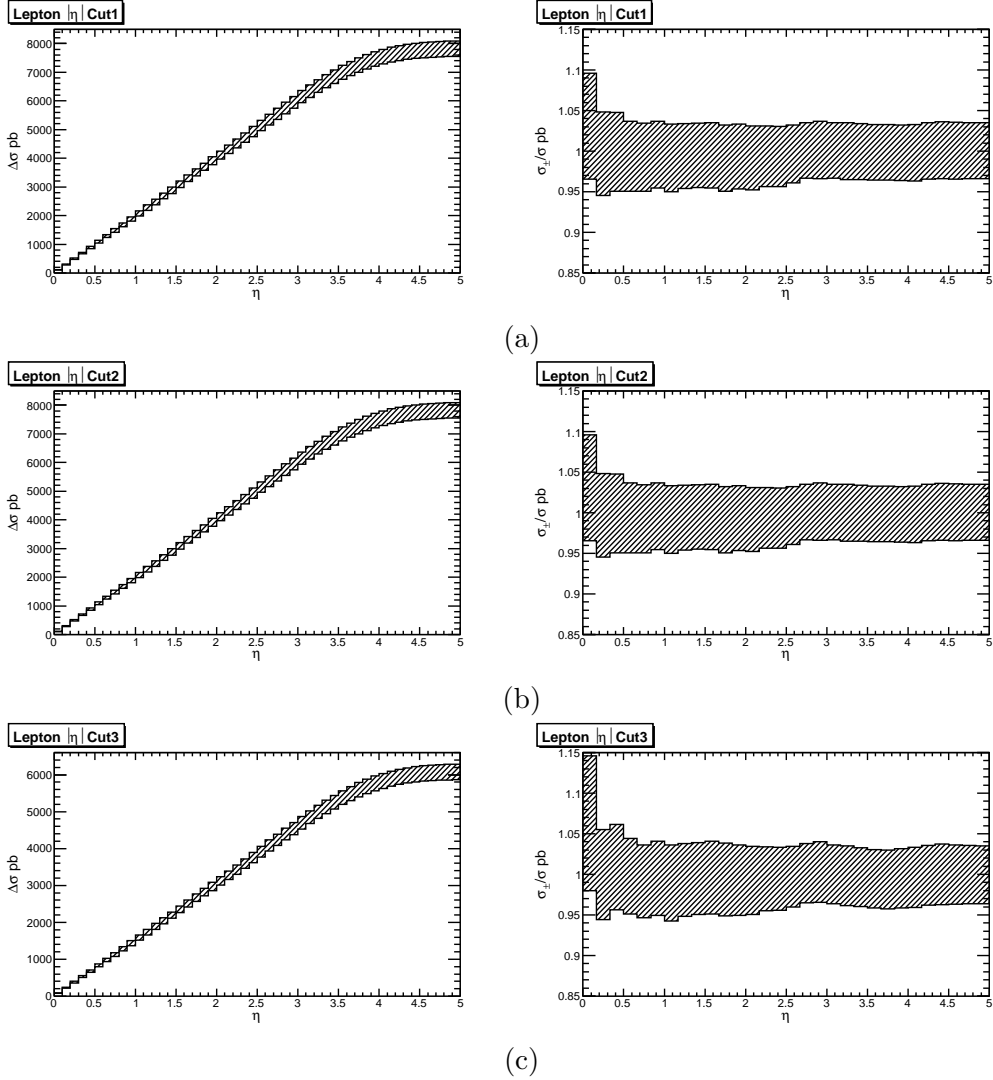


Figure 20: The $W^+ \rightarrow l^+\nu$ cross-section σ ($\ell = e$ or μ), as a function of the $|\eta|$ cut for acceptance regions (a) Cut 1, (b) Cut 2, and (c) Cut 3, as defined in Table 1. For each acceptance region we fix the invariant mass and p_T cuts at their specified values, and vary only the $|\eta|$ cut. The figures on the right show the relative errors in the cross sections.

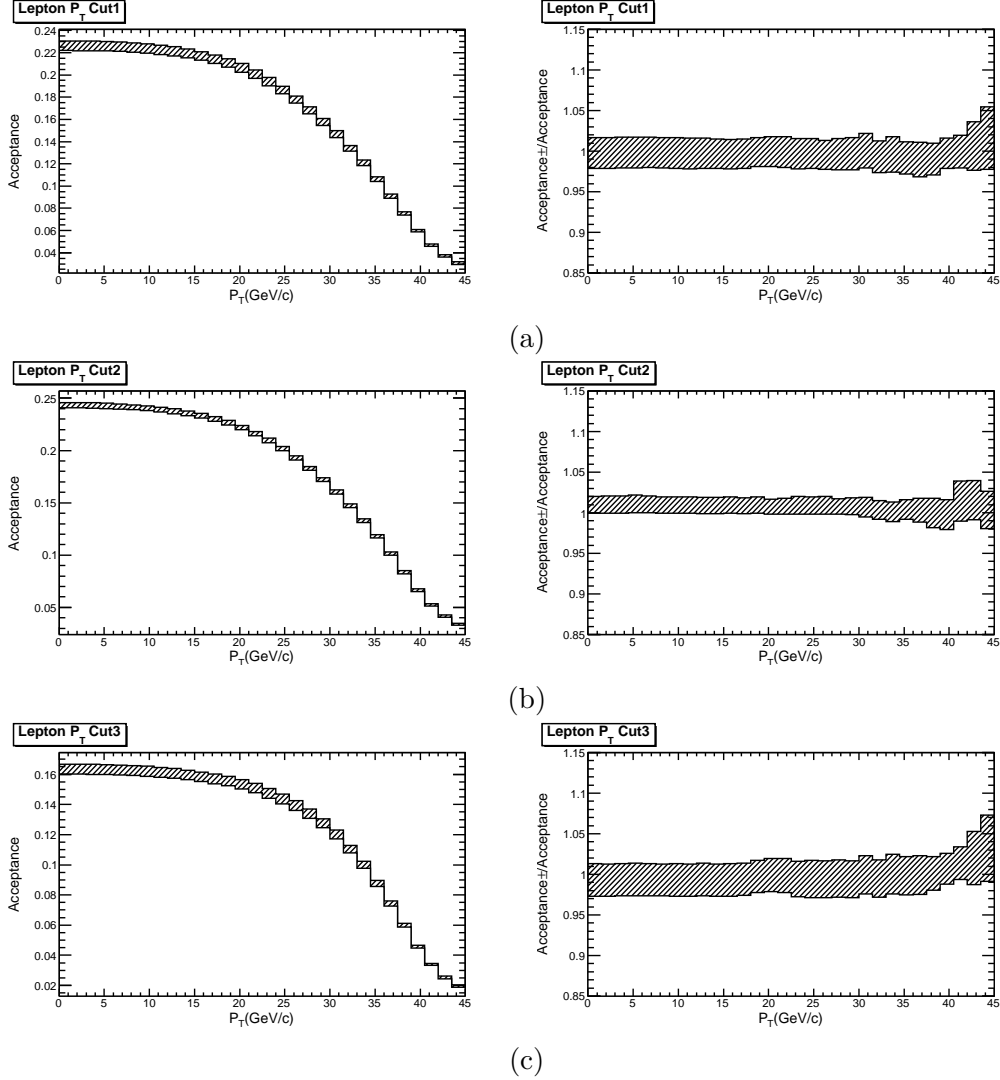


Figure 21: The $W^- \rightarrow l^- \bar{\nu}$ acceptances ($l = e$ or μ) A , as a function of the p_T cut for acceptance regions (a) Cut 1, (b) Cut 2, and (c) Cut 3, as defined in Table 1. For each acceptance region we fix the missing energy and $|\eta|$ cuts at their specified values, and vary only the p_T cut. The figures on the right show the relative errors in the acceptances.

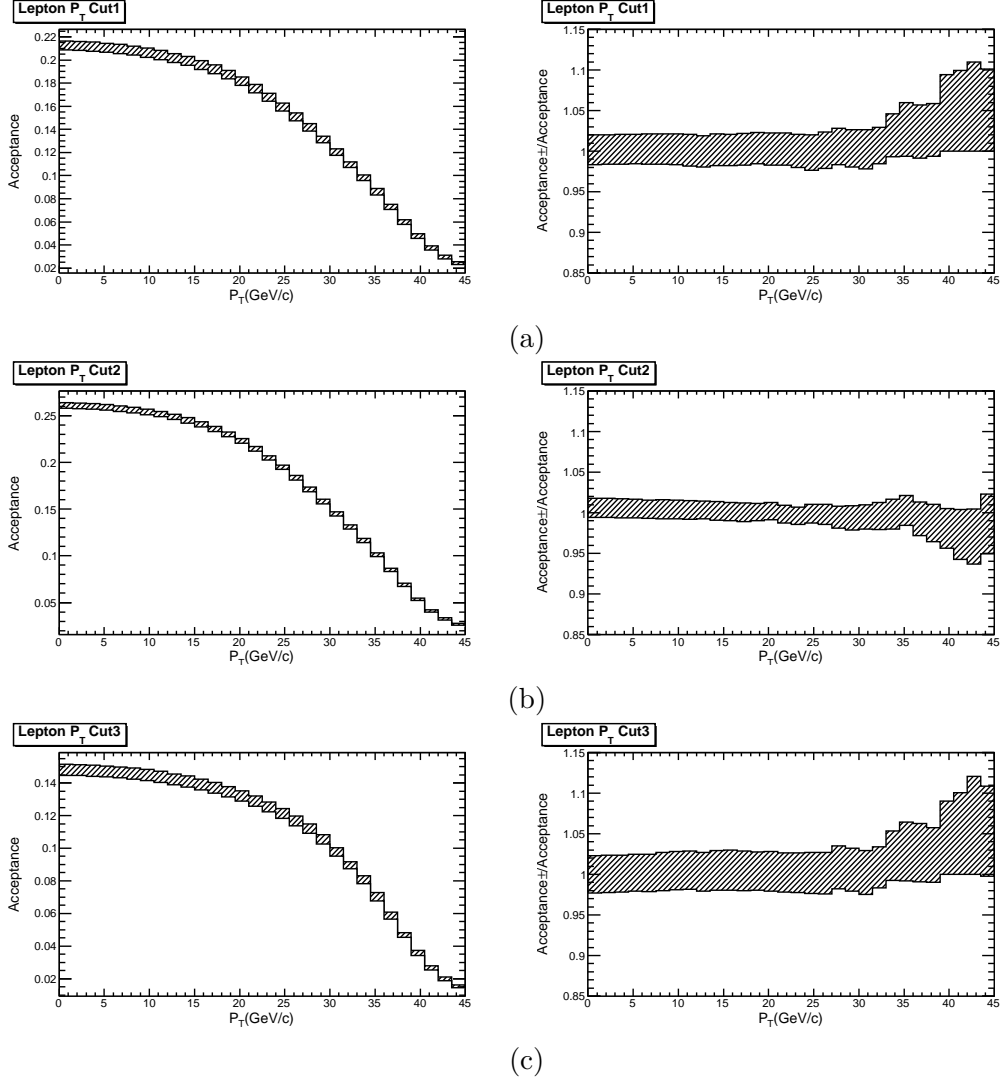


Figure 22: The $W^+ \rightarrow l^+ \nu$ acceptances ($\ell = e$ or μ) A , as a function of the p_T cut for acceptance regions (a) Cut 1, (b) Cut 2, and (c) Cut 3, as defined in Table 1. For each acceptance region we fix the missing energy and $|\eta|$ cuts at their specified values, and vary only the p_T cut. The figures on the right show the relative errors in the acceptances.

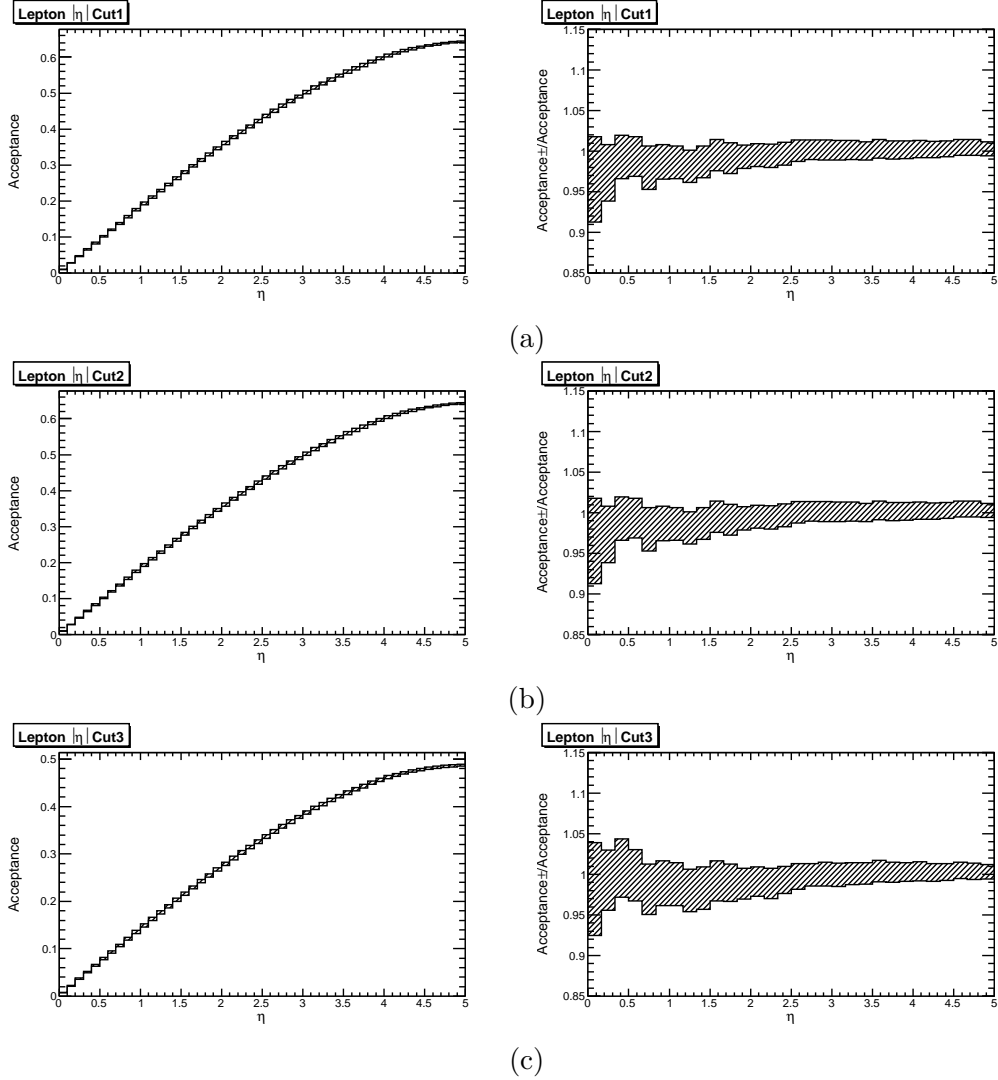


Figure 23: The $W^- \rightarrow l^- \bar{\nu}$ acceptances ($l = e$ or μ) A , as a function of the $|\eta|$ cut for acceptance regions (a) Cut 1, (b) Cut 2, and (c) Cut 3, as defined in Table 1. For each acceptance region we fix the missing energy and p_T cuts at their specified values, and vary only the $|\eta|$ cut. The figures on the right show the relative errors in the acceptances.

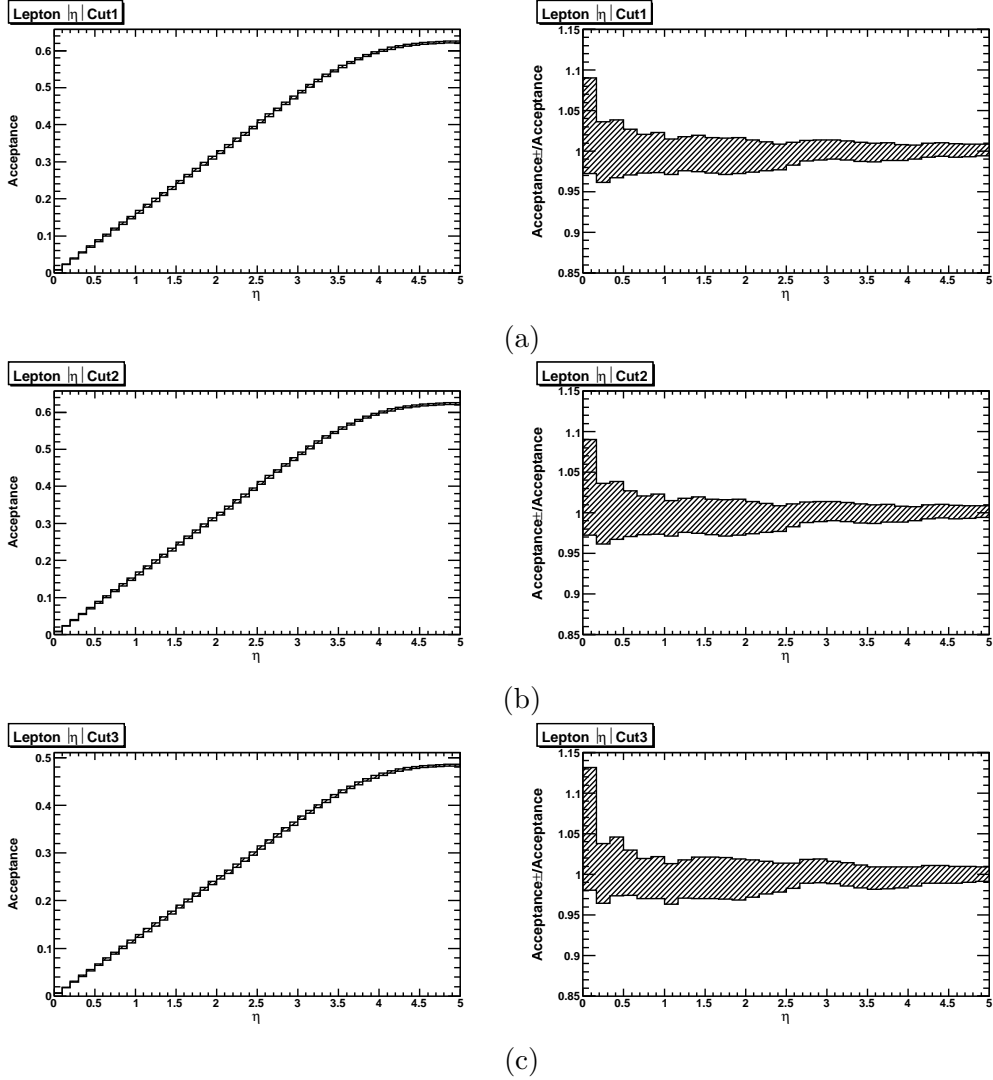


Figure 24: The $W^+ \rightarrow l^+ \nu$ acceptances ($\ell = e$ or μ) A , as a function of the $|\eta|$ cut for acceptance regions (a) Cut 1, (b) Cut 2, and (c) Cut 3, as defined in Table 1. For each acceptance region we fix the missing energy and p_T cuts at their specified values, and vary only the $|\eta|$ cut. The figures on the right show the relative errors in the acceptances.

References

- [1] M. Dittmar, F. Pauss and D. Zurcher, *Phys. Rev.* **D56** (1997) 7284 [hep-ex/9705004]; V.A. Koze, A.D. Martin, R. Orava and M.G. Ryskin, *Eur. Phys. J.* **C19** (2001) [arXiv:hep-ph/0010163]; W.T. Giele and S.A. Keller, arXiv:hep-ph/0104053;
- [2] M.W. Krasny, F. Fayette, W. Placzek, *Eur. Phys. J.* **C51** (2007) 607.
- [3] N.E. Adam, V. Halyo and S.A. Yost, *JHEP* **05** (2008) 062 [arXiv:0802.3251].
- [4] S. Frixione and M.L. Mangano, *JHEP* **0405** (2004) 056 [arXiv:hep-ph/0405130].
- [5] R. Hamburg, W.L. van Neerven and T. Matsuura, *Nucl. Phys.* **B359** (1991) 343 [Erratum: *ibid.* **B644** (2002) 403]; R.V. Harlander and W.B. Kilgore, *Phys. Rev. Lett.* **88** (2002) 201801 [arXiv:hep-ph/0201206].
- [6] C. Anastasiou, L. Dixon, K. Melnikov, and F. Petriello, *Phys. Rev. Lett.* **91** (2003) 182002; *Phys. Rev.* **D69** (2004) 094008 [arXiv:hep-ph/0312266]; www.slac.stanford.edu/~lance/Vrap/.
- [7] K. Melnikov and F. Petriello, *Phys. Rev. Lett.* **96** (2006) 231803 [arXiv:hep-ph/0603182], *Phys. Rev.* **D74** (2006) 114017 [arXiv:hep-ph/0609070]; www-d0.fnal.gov/d0dist/dist/packages/melnikov_petriello/devel/FEHP.html.
- [8] S.D. Drell and T.M. Yan, *Phys. Rev. Lett.* **25** (1970) 316.
- [9] M. Bertini, L. Lönnblad, and T. Sjöstrand, *Comput. Phys. Commun.* **134** (2001) 365; T. Sjöstrand, P. Edén, C. Friberg, L. Lönnblad, G. Miu, S. Mrenna and E. Norrbin, *Comput. Phys. Commun.* **135** (2001) 238; T. Sjöstrand, L. Lönnblad, S. Mrenna, and P. Skands, arXiv:hep-ph/0308153; T. Sjöstrand, S. Mrenna, and P. Skands, arXiv:hep-ph/0603175; www.thep.lu.se/~torbjorn/Pythia.html.
- [10] G. Marchesini, B.R. Webber, G. Abbiendi, I.G. Knowles, M.H. Seymour and L. Stanco, *Comp. Phys. Commun.* **67** (1992) 465; G. Corcella, I.G. Knowles, G. Marchesini, S. Moretti, K. Odagiri, P. Richardson, M.H. Seymour and B.R. Webber, *JHEP* **0101** (2001) 010 [arXiv:hep-ph/0011363]; arXiv:hep-ph/0210213; S. Gieseke, A. Ribon, M.H. Seymour, P. Stephens and B. Webber, *JHEP* **0402**, 005; hepwww.rl.ac.uk/theory/seymour/herwig/.
- [11] H. Baer, F.E. Paige, S.D. Protopopescu, and X. Tata, arXiv:hep-ph/0312045; www.phy.bnl.gov/~isajet/.
- [12] T. Gleisberg, S. Höche, F. Krauss, A. Schälicke, S. Schumann, and J.C. Winter, *JHEP* **0402** (2004) 056; A. Schaelicke and F. Krauss, *JHEP* **0507** (2005) 018; F. Krauss, A. Schaelicke, S. Schumann, G. Soff, *Phys. Rev.* **D72** (2004) 114009; *ibid.* (2005) 054017; projects.hepforge.org/sherpa/dokuwiki/doku.php.
- [13] B.I. Ermolaev and V.S. Fadin, *LETP Lett.* **33** (1981) 269; A.H. Mueller, *Phys. Lett.* **B104** (1981) 161; A. Bassetto, M. Ciafaloni, G. Marchesini, and A.H. Mueller, *Nucl. Phys.* **B207** (1982) 189; V.S. Fadin, *Yad. Fiz.* **37** (1983) 408; F. Abe *et al.*, *Phys. Rev.* **D50** (1994) 5562; B. Abbot *et al.*, *Phys. Lett.* **B414** (1997) 419.
- [14] R.K. Ellis, D.A. Ross and S. Veseli, *Nucl. Phys.* **B503** (1997) 309.
- [15] S. Frixione and B.R. Webber, *JHEP* **0206** (2002) 029 [arXiv:hep-ph/0204244]; S. Frixione, P. Nason and B.R. Webber, *JHEP* **0308** (2003) 007 [arXiv:hep-ph/0305252]; www.hep.phy.cam.ac.uk/theory/webber/MCatNLO/.

- [16] E. Barberio, B. van Eijk, and Z. Wąs, *Comput. Phys. Commun.* **66** (1991) 115; E. Barberio and Z. Wąs, *Comput. Phys. Commun.* **79** (1994) 291; P. Golonka and Z. Wąs, *Eur. Phys. J.* **C45** (2006) 97; wasm.web.cern.ch/wasm/goodies.html; P. Golonka and Z. Wąs, *Eur. Phys. J.* **C50** (2007) 53.
- [17] N.E. Adam, C.M. Carloni Calame, V. Halyo and C. Shepherd-Themistocleous
“Comparison of HORACE and PHOTOS in the $Z \rightarrow \ell^+\ell^-$ Peak Region” to appear in Les Houches Proceeding.
- [18] C.M. Carloni Calame, G. Montagna, O. Nicrosini and M. Treccani, *Phys. Rev.* **D69** (2004) 037301; *JHEP* **0505** (2005) 019; C.M. Carloni Calame, G. Montagna, O. Nicrosini and A. Vicini, *JHEP* **0612** (2006) 016; *JHEP* **10** (2007) 109; www.pv.infn.it/~hepcomplex/horace.html.
- [19] G. Balossini, G. Montagna, C.M. Carloni Calame, M. Moretti, M. Treccani, O. Nicrosini, F. Piccinini, and A. Vicini, arXiv:0805.1129; PoS (RAD COR 2007) 013; *Acta Phys. Polon.* **B38** (2007) 3407; C.M. Carloni Calame, G. Montagna, O. Nicrosini, F. Piccinini, and A. Vicini, *AIP Conf. Proc.* **870** (2006) 436.
- [20] Q.-H. Cao and C.-P. Yuan, *Phys. Rev. Lett.* **93** (2004) 042001; C. Balázs and C.-P. Yuan, *Phys. Rev.* **D56** (1997) 5558; C. Balázs, J.-W. Qiu and C.-P. Yuan, *Phys. Lett.* **B355** (1995) 548; G.A. Ladinsky and C.-P. Yuan, *Phys. Rev.* **D50** (1994) 4239; hep.pa.msu.edu/resum/.
- [21] U. Baur, S. Keller, and W.K. Sakumoto, *Phys. Rev.* **D57** (1998) 199; U. Baur, O. Brein, W. Hollik, C. Schappacher, and D. Wackerroth, *Phys. Rev.* **D65** (2002) 033007.
- [22] W.K. Tung, H.L. Lai, A. Belyaev, J. Pumplin, D. Stump, C.-P. Yuan, *JHEP* **0702** (2007) 053; D. Stump, J. Huston, J. Pumplin, W.-K. Tung, H.L. Lai, S. Kuhlmann, and J.F. Owens, *JHEP* **0310** (2003) 046; J. Pumplin, D. Stump, J. Huston, H.L. Lai, P. Nadolsky and W.-K. Tung, *JHEP* **07** (2002) 012; hep.pa.msu.edu/people/wkt/cteq6/cteq6pdf.html.
- [23] C. Anastasiou, K. Melnikov, and F. Petriello, *Nucl. Phys.* **B724** (2005) 197; *Phys. Rev. Lett.* **93** (2004) 262002; *ibid.* 032002.
- [24] G.P. Lepage, *J. Comp. Phys.* **27** (1978) 192; T. Hahn, *Comput. Phys. Commun.* **168** (2005) 78.
- [25] A.D. Martin, R.G. Roberts, W.J. Stirling, and R.S. Thorne, *Phys. Lett.* **B652** (2007) 292, *ibid.* **B636** (2006) 259; *Eur. Phys. J.* **C28** (2003) 455, *ibid.* **C23** (2002) 73, *ibid.* **C18** (2000) 117; durpdg.dur.ac.uk/hepdata/mrs.html.
- [26] A. Cafarella, C. Coriano, and M. Guzzi, *JHEP* **0708** (2007) 030; *Nucl. Phys.* **B748** (2006) 253.
- [27] C. Glosser, S. Jadach, B.F.L. Ward, and S. Yost, *Mod. Phys. Lett.* **A19** (2004) 2113; *Int. J. Mod. Phys.* **A20** (2005) 3258; B.F.L. Ward and S.A. Yost, *Acta Phys. Polon.* **B38** (2007) 2395; arXiv:0802.0724 [hep-ph].